Journal of Archaeological Science 181 (2025) 106330

Contents lists available at ScienceDirect

Journal of Archaeological Science

journal homepage: www.elsevier.com/locate/jas

Built-in smartphone LiDAR for archaeological and speleological research

Daniel Antón [a,b,*], Juan Mayoral-Valsera [c,d], María Dolores Simón-Vallejo [d,e], Rubén Parrilla-Giráldez [d,f], Miguel Cortés-Sánchez [d,e]

[a] Departamento de Expresión Gráfica e Ingeniería en la Edificación, Escuela Técnica Superior de Ingeniería de Edificación, Universidad de Sevilla, Seville, 41012, Spain
[b] Product Innovation Centre and The Creative and Virtual Technologies Research Lab, School of Architecture, Design and the Built Environment, Nottingham Trent University, Nottingham, NG1 4FQ, UK
[c] Grupo Espeleológico Plutón, Spain
[d] HUM1089-PAMSUR Project, Spain
[e] Departamento de Prehistoria y Arqueología, Facultad de Geografía e Historia, Universidad de Sevilla, Seville, 41004, Spain
[f] ICArEHB, Universidade do Algarve, Portugal

ARTICLE INFO

Keywords:
Mobile LiDAR
Terrestrial laser scanning
3D model accuracy
Prehistoric Art
Archaeology
Speleology

ABSTRACT

LiDAR technology is reshaping cave surveying by providing detailed 3D models that enhance the accuracy of morphological and rock art digitisation and reduce subjective interpretation. This technology, in its varied forms and solely or combined with other remote sensing techniques such as photogrammetry, enriches the documentation and supports multidisciplinary research by enabling spatial analyses and virtual exploration, thus opening new possibilities in various fields such as archaeology, geology, speleology, tourism or education. In this sense, this research aimed to democratise the use of low-cost mobile LiDAR (Light Detection and Ranging) 3D scanning, subjected to fewer accessibility limitations than tripod-mounted Terrestrial Laser Scanners (TLS), in cave archaeology and speleology. For this purpose, La Pileta Cave in Málaga (Spain) was chosen as a case study. Declared a Spanish National Monument in 1924, the cave boasts one of the greatest collections of prehistoric art in Europe and, therefore, a reference in South Iberia, and outstands out for its varied karstic morphologies. The research methodology involved a systematic process to ensure clarity and accuracy. First, the main itinerary in La Pileta was scanned using the smartphone LiDAR technique. This was followed by a Terrestrial Laser Scanning (TLS) survey of a specific sector within the same itinerary, with numerous morphological details of its karstic environment and important Palaeolithic rock art samples. Both the smartphone LiDAR and TLS spatial data were then validated against a Ground Control Points (GCPs) network previously established using a total station. Given the higher accuracy of TLS for graphical documentation, it was further employed as a benchmark to validate the accuracy of smartphone LiDAR. Despite its limitations, this research revealed smartphone LiDAR as a suitable technique for geometric data recording in cave archaeology and speleology. Solely or combined with TLS, mobile LiDAR can be used to document rock art panels in karstic environments, surpassing the latter technique in terms of texture quality. In addition to the accurate graphic documentation carried out in the cave sector, this research broke down the advantages and disadvantages of the smartphone LiDAR technique and provided a series of recommendations for its use in this context.

1. Introduction

Recent technological advancements have transformed archaeology and speleology through three-dimensional (3D) digitisation and visualisation techniques (Remondino and Campana, 2014; Cortes-Sánchez et al., 2017; Ruiz López and Viñas i Vallverdú, 2020; Arias et al., 2022). Accurately documenting archaeological sites and cave systems has traditionally been difficult due to their morphological complexity and limited accessibility. Conventional methods, while established, often lack the spatial resolution and detail necessary for comprehensive scientific analysis and long-term conservation strategies. Today, remote sensing technologies improve the documentation and management of heritage sites and objects (Lerma et al., 2010; Kartini et al., 2024).

3D scanning and photogrammetry are established geometry capture

* Corresponding author. Departamento de Expresión Gráfica e Ingeniería en la Edificación, Escuela Técnica Superior de Ingeniería de Edificación, Universidad de Sevilla, Seville, 41012, Spain.
E-mail address: danton@us.es (D. Antón).

https://doi.org/10.1016/j.jas.2025.106330
Received 3 April 2025; Received in revised form 3 July 2025; Accepted 19 July 2025
Available online 7 August 2025

techniques in architecture and cultural heritage. Terrestrial Laser Scanning (TLS) is known for its high accuracy and ability to generate detailed spatial datasets, particularly in geometrically complex and sometimes inaccessible cave environments (Lerma et al., 2010; Kartini et al., 2024). It measures the time it takes for laser pulses to return from surfaces, creating a point cloud of millions of coordinates (Bakker et al., 2009). However, TLS's limitations include high costs and equipment size (Antón et al., 2024a), making it less accessible for smaller projects and challenging cave environments (Giordan et al., 2021). The distances and angles also impact survey accuracy (Tan and Cheng, 2017; Tan et al., 2018). To address these issues, more flexible alternatives, e.g., backpack and handheld LiDAR (Light Detection and Ranging) systems, including smartphone LiDAR, have been effectively utilised in geological and cultural heritage studies (Liu et al., 2024; Özdemir et al., 2022; Šupinský et al., 2022).

Structure-from-Motion (SfM) photogrammetry, a more accessible alternative, needs a camera and specific software to capture multiple photographs of an object from different angles to match feature points and calculate the camera's position and orientation for 3D scene reconstruction through triangulation (Jiang et al., 2020; Özyeşil al., 2017). SfM is relatively inexpensive and effective, producing detailed and photorealistic models, but it requires references to align and scale the model and considerable post-processing effort and time for accuracy. This technique also faces limitations in low-light cave environments where texture features may be insufficient (Lerma et al., 2010; Kartini et al., 2024).

Integrating LiDAR sensors in smartphones has made 3D scanning more accessible. While extensive data capture technologies offer higher accuracy, smartphone LiDAR ensures portability, affordability, and ease of use (Luetzenburg et al., 2021; Fiorini, 2022). Smartphone LiDAR requires minimal technical expertise for its operation to produce textured 3D meshes in real time (Wang et al., 2025). Overall, mobile LiDAR technology can facilitate detailed digital replicas and documentation in caves, vital for heritage study and conservation. However, the accuracy of these mesh data requires further assessment, especially for archaeological and speleological applications where morphological detail and measurement precision are critical. Therefore, this research addresses this knowledge gap by conducting a comprehensive accuracy assessment of built-in smartphone LiDAR technology. For this purpose, La Pileta Cave in Benaoján, Málaga (Spain), is used as a demanding test case that combines exceptional prehistoric art with complex karstic morphologies.

The rest of this paper is structured as follows: Section 2 reviews the literature on computer vision in archaeology and cave exploration, focusing on digitisation and modelling technologies. Section 3 outlines the research aim and objectives. Section 4 describes the materials and methodology adopted, which consists of geometry data capture and triangulation, as well as the validation of the techniques used. Sections 5 and 6 present the results and discussion. Finally, Section 7 (Conclusions) brings together research implications and the benefits and downsides of smartphone mobile LiDAR and provides recommendations for its use in cave archaeology and speleology.

1.1. La Pileta cave

Prehistoric art represents one of the earliest expressions of complex human symbolism. Initial debate about its existence in Palaeolithic context determined its French-Cantrabian distribution (Cortes-Sánchez et al., 2023). However, shortly afterwards, the La Pileta Cave (South Spain), was discovered outside the consensus rock art area. This complex karstic system containing Paleolithic graphics was initially studied by Breuil et al., in 1915 (Breuil et al., 1915), marking the beginning of the pan-European dimension of the rock art phenomenon. This relevance led to its being reported in journals such as Nature (Wright, 1916), among others, or exhibited at the Royal Society of London (Smith, 2009).

Declared a Spanish National Monument in 1924 (Decreto 527, 1996), La Pileta Cave stands as one of the most remarkable rock art sites in Europe, distinguished by both the quality and diversity of its preserved graphic horizons. The cave contains an extraordinary inventory of 1236 motifs, with 872 attributed to Paleolithic art and 364 to post-Paleolithic schemas (Sanchidrián Torti and Muñoz Vivas, 1990; Medina Alcaide et al., 2015), with ongoing research continuing to reveal additional motifs (Simon-Vallejo et al., 2021, 2024). These graphic traces span approximately 30,000 years from the Upper Paleolithic through the Bronze Age, making it one of the sites with the greatest quantity and variety of graphic motifs (Jordá Cerdá, 1955; Cortes-Sánchez et al., 2016a).

The first presentation of La Pileta's prehistoric art was conducted by Henri Breuil and collaborators (1915) (Breuil et al., 1915), who proposed two major phases: a Paleolithic phase distributed across three artistic cycles represented by three different colorations (yellow, red, and black pigments), and a second phase framed within Recent Prehistory. This pioneering work also provided the first topography of the cave.

In the 1970s, Lya and Marcel Dams studied the cavity during three campaigns and published various works. Notwithstanding, some of their graphic interpretations and panel analyses were later questioned, thus limiting their use in subsequent historiography (Dams and Dams, 1975, 1977a, 1977b, 1983). Other partial revisions of La Pileta's Paleolithic rock art were carried out by Francisco Jordá Cerdá (1955) (Jordá Cerdá, 1955), Eduardo Ripoll Perelló (1957, 1962) (Ripoll Perello, 1957; Ripoll Perelló and de Mergelina y Luna, 1962), and Javier Fortea Pérez et al. (2005) (Fortea Pérez et al., 2005).

After that, the research carried out by J.L. Sanchidrián Torti aimed to organise the chronology of paintings, proposing a seriation composed of techno-stylistic "blocks" and "horizons", framing the Paleolithic manifestations between the Solutrean and Magdalenian periods. This work also obtained the only current radiocarbon date from an auroch paint (20,130 ± 350 BP) (Sanchidrián Torti and Muñoz Vivas, 1990, 1991; Medina Alcaide et al., 2015; Sanchidrián Torti, 1985, 1986; Sanchidrián Torti et al., 1997, 2001).

Current research, developed over the last ten years, has consolidated the possibility of pre-Solutrean graphic assemblages in La Pileta based on new developments in the chronocultural sequence of the ancient Upper Paleolithic in southern Iberia. This hypothesis is supported by the identification of positive hand representations in different cave chambers (Simón-Vallejo et al., 2024; Cortes-Sánchez et al., 2015) and pigments adhered to a lamp probably used during Gravettian times (Cortes-Sánchez et al., 2016b), representing one of the oldest known illumination devices in the Iberian Peninsula and also in different studies from the same geographical area (Cortes-Sánchez et al., 2018a, 2019).

The cave has also been the subject of specific studies on Neolithic materials (Cortes-Sánchez and Simón-Vallejo, 2007), newly discovered hand representations (Simón-Vallejo et al., 2024; Cortes-Sánchez et al., 2015), historical analysis (Cortes-Sánchez et al., 2023), and new zoomorphs and panels (Simón-Vallejo et al., 2024). Current research focuses on renewing all graphic documentation for the cave and exploring and digitising cave topography with modern instruments and methodologies (Mayoral Valsera et al., 2017; Mayoral Valsera, 2020; Parrilla Giráldez, 2023).

The archaeological sequence of La Pileta includes evidence from excavations by Obermaier in the "Sala de las Vacas" and "Sala de Murciélagos", later expanded in 1942 by Giménez Reyna (Giménez Reyna et al., 1958; Giménez Reyna, 1951, 1958). Although material preservation is limited, diagnostic elements suggest a sequence encompassing at least Middle Paleolithic, Upper Paleolithic (Gravettian, Solutrean, and Magdalenian), Neolithic, Chalcolithic, and Bronze Age periods, representing a continuous human presence spanning from Neanderthal to Bronze Age times (Cortes-Sánchez and Simón-Vallejo, 2007).

In recent years, the comprehensive research program have been developed to achieve a more holistic and profound understanding of La

Table 1
Estimated comparison between relevant smartphone LiDAR and TLS equipment and software.

Technology	Equipment cost (€)	Software cost (€)
Terrestrial Laser Scanners	20,000–80,000	1000–10,000
Apple 'Pro' mobile devices	900–1600	0–350

Source: Own elaboration.

Pileta, encompassing both rock art and archaeological records and 3D topography (Mayoral Valsera et al., 2017; Mayoral Valsera, 2020; Parrilla Giráldez, 2023). This integral investigation of the cavity continues to yield new discoveries and insights, solidifying La Pileta's position as one of Europe's most significant prehistoric art sites and a crucial location for understanding the development of human complex symbolism.

La Pileta is an extraordinary heritage site, recognised not only for its rock art but also for the distinctive shapes present in its karst formations. However, its documentation has so far been limited to conventional topographical methods. Consequently, this karstic environment has yet to be extensively digitised using modern technology, which, in turn, offers the opportunity to analyse and implement alternative geometry capture equipment.

From a topographical perspective, La Pileta represents an intricate karstic system along hitherto-explored 2.5 km of galleries, which present significant documentation challenges (Mayoral Valsera et al., 2017; Mayoral Valsera, 2020). Some of the most distinguished researchers on prehistoric art have studied the graphic manifestations of La Pileta, but without a scientific topography meeting its archaeological and heritage documentation needs. Thus, La Pileta Cave has been explored and documented, albeit not entirely or with millimetric precision. A significant advancement occurred when speleologists and archaeologists employed the Disto X2 laser metre and Topodroid software, drew a plan of the known system, which supported the development of the so-called *hybrid system of speleological topography* (Mayoral Valsera et al., 2017; Mayoral Valsera, 2020). This first 3D model of La Pileta had a higher resolution than those produced using traditional techniques, representing a crucial step forward in cave documentation. However, despite these advances, the resulting models lacked the morphological detail necessary for comprehensive karstic shape representation and high-quality texture mapping of rock art panels.

This technological and documentation gap presents an exceptional opportunity to evaluate smartphone LiDAR technology in a demanding real-world scenario that combines complex cave morphologies with internationally significant prehistoric art assemblages. The methodological assessment conducted in La Pileta's challenging environment provides crucial insights into the potential of mobile 3D scanning technologies for archaeological and speleological applications.

2. State of the art

Digital documentation technologies have transformed how researchers capture and interpret spatial data in archaeology, architecture, and cultural heritage. These digitisation technologies create detailed digital models, enhancing the conservation of fragile and complex environments and enabling accurate analysis without physical interference (European Commission's Expert Group on Digital Cultural Heritage and Europeana (DCHE Expert Group), 2020). For instance, airborne LiDAR helped discover cave entrances in heavily forested areas (Moyes and Montgomery, 2019), and mobile SLAM-based LiDAR offers rapid field coverage and contextual efficiency, albeit with reduced accuracy (approximately 1 cm) and susceptibility to drift in feature-sparse environments (Shao et al., 2019). Remote sensing and visualisation also open new opportunities for public engagement, educational activities, and accessibility in both public property and heritage contexts (Antón et al., 2024b; Pietroni et al., 2023). Combining various digital documentation methods, especially TLS and SfM, improves surface and texture data quality by overcoming the limitations of individual technologies (Gines and Cervera, 2020; Ulvi, 2021; Balestrieri et al., 2024; Alshawabkeh and Baik, 2023; Tysiac et al., 2023). However, the recent introduction of built-in LiDAR sensors in smartphones has opened a new digitisation paradigm in caves, offering greater manoeuvrability and overcoming the operational constraints of traditional methods.

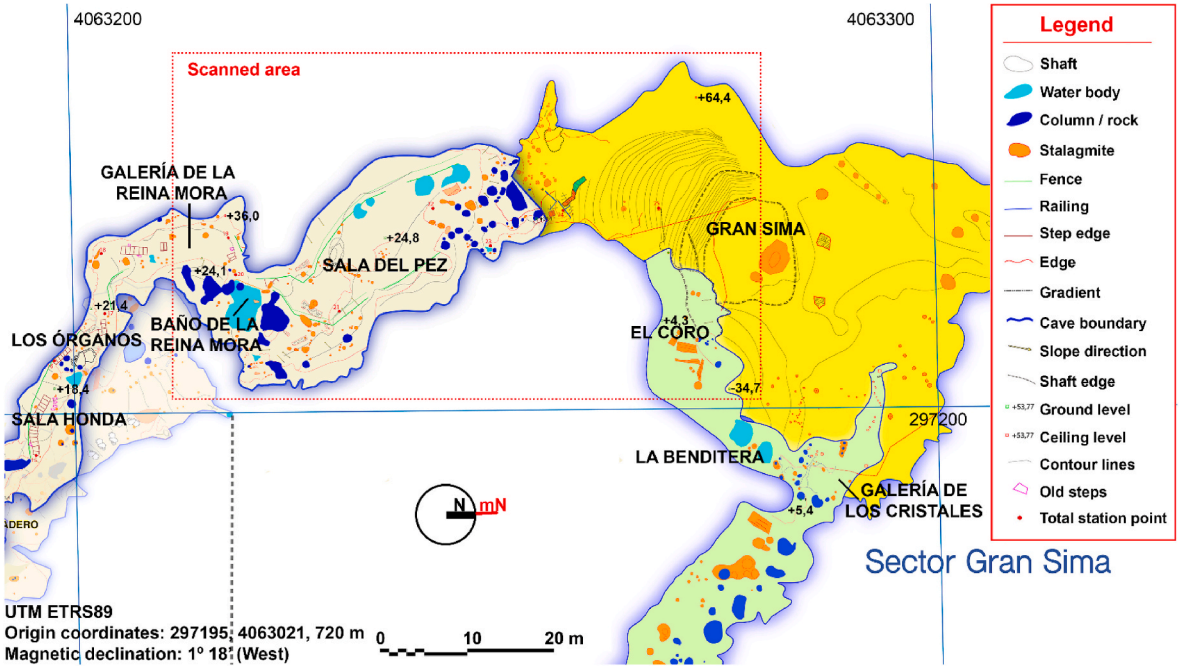

Fig. 1. Cave sector surveyed.
Source: Own elaboration based on Juan Mayoral-Valsera's map of La Pileta (Mayoral Valsera et al., 2017).

Fig. 2. Smartphone LiDAR scanning in La Pileta.
Source: Photograph taken by Sandro Téllez, Sociedad Espeleológica Marbellí.

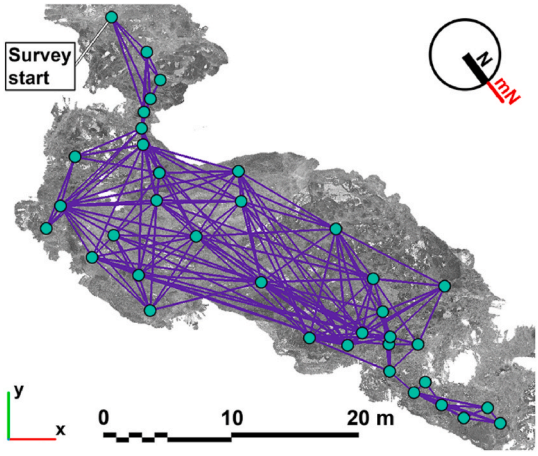

Fig. 3. 3D survey layout: TLS stations and scan links. Top view.
Source: Own elaboration.

2.1. Leading digitisation technologies

Widely used for high-accuracy 3D documentation, TLS produces dense point clouds with millimetre precision, ideal for complex cave environments. By extracting floor geometry from TLS clouds, Šupinský et al. (2022) used 3D mesh shading to enhance cave cartography and represented cave features. Geographic Information Systems (GIS) can further analyse cave scans: Liu et al. (2024) imported TLS data into GIS to study cave heights and elevation flows, utilising Simultaneous Localisation and Mapping (SLAM) mobile LiDAR for real-time data registration. Similarly, Lozano Bravo et al. (Lozano Bravo et al., 2023) digitised a large cave using handheld and drone-mounted SLAM and segmented the cave floor to produce a site map in a GIS.

Combining LiDAR with other technologies has facilitated comprehensive cave studies, enhancing data accuracy and texture quality and enabling morphometric analysis, geological investigations, and rock art and cave morphology documentation and understanding (Lerma et al., 2010). This integration enables the detailed documentation of complex cave systems where traditional survey methods are impractical. Early research in cave archaeology focused on accurate geometric documentation. González-Aguilera et al. (2009) established a multi-sensor approach with TLS and digital photography to document Palaeolithic art. Hoffmeister et al. (2016) enhanced LiDAR data incorporating RGB values and lighting simulations in the Ardales Cave. Pepe et al. (2021) conducted data fusion in a challenging scenario with poor lighting conditions. Çömert et al. (2023) combined TLS and Unmanned Aerial Vehicle (UAV) photogrammetry for accurate documentation of Turkish cave systems and used GIS for risk assessment. Using those remote sensing techniques, Zhang et al. (2024) captured a cave site's indoor and outdoor geometry with accuracies above 40 mm and 20 mm, and Pukanská et al. (2020) documented the structure and intricate details of the Ochtiná Aragonite Cave (Slovakia). Structured-Light Scanning (SLS) projects grid light patterns (grids of light points) onto a surface and, through triangulation, reconstructs sub-millimetre, high-density 3D geometry (3D meshes with up to 0.1 mm point accuracy and 0.2 mm resolution (Artec 3D, 2017)). A Red-Green-Blue (RGB) camera integrated in the SLS device provides the colour to map textures on those 3D meshes. Hybrid SLS systems often incorporate a Time-of-Flight (ToF) depth sensor (a type of depth camera) which provides rapid coarse ranging over larger areas, while SLS refines critical zones for accuracy. This results in a depth map with both high density and global coverage, and colour texture mapped from the device's camera. Consequently, these handheld systems integrate real-time geometry and texture tracking, offering live feedback, onboard processing (Leo), and high-quality colour mapping via integrated cameras. They are suitable for medium-to-large heritage artefacts and surfaces, but imply working distances of 0.35–1 m and can struggle with glossy or transparent materials without surface preparation. Considering the above description, specifications, capabilities, and limitations, SLS can complement TLS in architectural heritage. Its accurate meshes can integrate with 3D point clouds (Moyano et al., 2017) and TLS-based Historic Building Information Models (HBIM) (Barazzetti et al., 2015a; Simeone et al., 2014; Nieto et al., 2016; Oreni et al., 2013; Chiabrando et al., 2016; HichriStefani et al., 2013; Brumana et al., 2014; Murphy et al., 2009; Antón et al., 2018). The HBIM methodology is the application of Building Information Modelling (BIM)—a common technology in the AEC (Architecture, Engineering, and Construction) sector—to heritage, where three-dimensional geometry is constantly enriched with semantic, documentary and relational information (Bassier et al., 2020; Werbrouck et al., 2020; Xue et al., 2021). In this context, focusing on 3D geometries, SLS aids in, e.g., representation enhancement of complex elements, cataloguing, and digital replicas for restoration. SLS's sub-millimetre, high-polygon (commonly referred to as high-poly) surface meshes are suitable for capturing intricate details, whereas TLS, offering millimetre-to-centimetre accuracy and recording larger volumes in real-world coordinate systems, is susceptible to occlusions that may leave gaps in areas not directly visible to the scanner (Riquelme et al., 2017). The combination of both technologies enables a multi-scale data-fusion workflow. Likewise, research has also leveraged accurate remote sensing techniques such as UAV photogrammetry using

a)

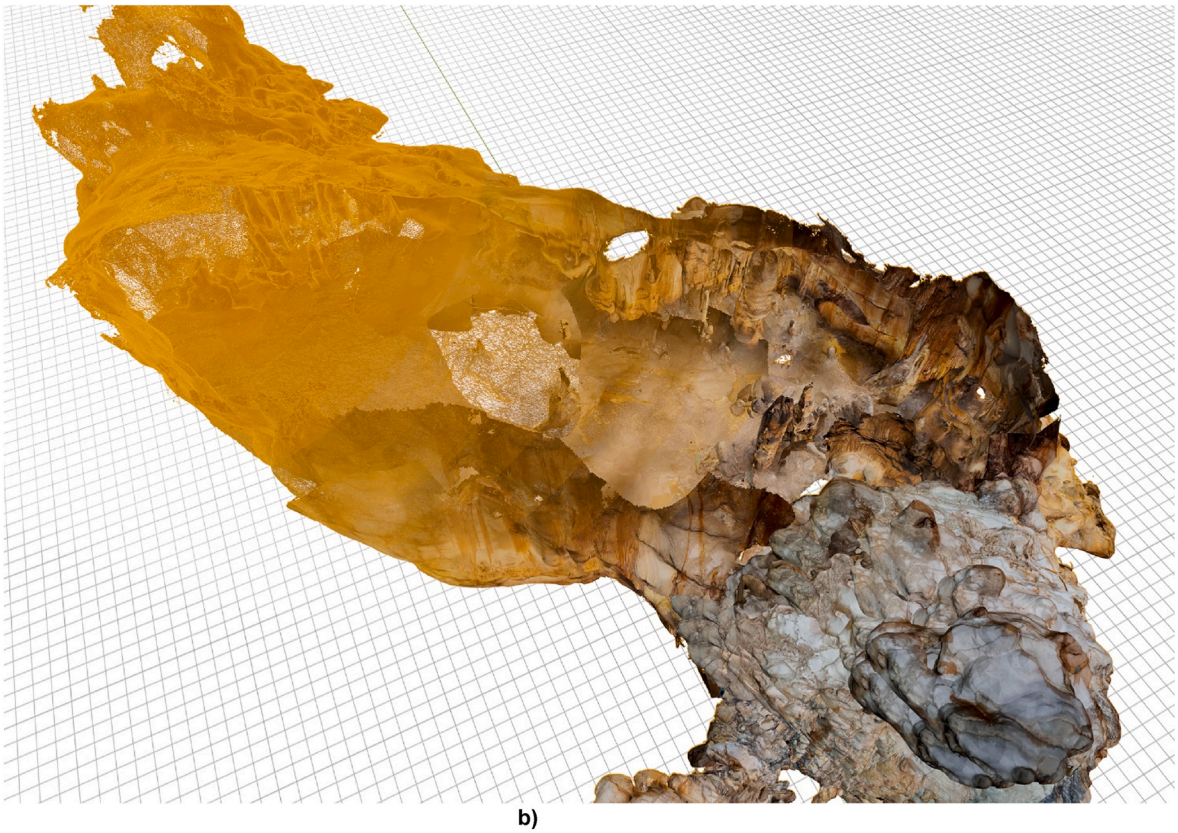

b)

Fig. 4. Mobile LiDAR output 3D mesh, from wireframe (left) to textured geometry (right): **a)** Gran Pez panel; **b)** Sala del Pez.
Source: Own elaboration.

millimetre-resolution cameras and micrometre-resolution SLS to record surface defects of concrete bridges to support structural health monitoring (Backhaus et al., 2024). In cave archaeology, Cortes-Sánchez et al. (2018b) created a TLS 3D mesh of a cavity and digitised rock engravings using SLS and SfM. Rivero et al. (2024) developed a mobile visualisation system for rock art panels using LiDAR, SLS, and SfM for public engagement and accessibility. They used tablet LiDAR for model positioning and photogrammetric texture mapping onto SLS geometry, overlaying it with prehistoric drawings. However, SLS's high accuracy implies large 3D meshes, impeding extensive cave digitisation with current hardware. Given their limited range, expensive SLS devices can capture partial site geometries; they need extensive scaffolding to avoid

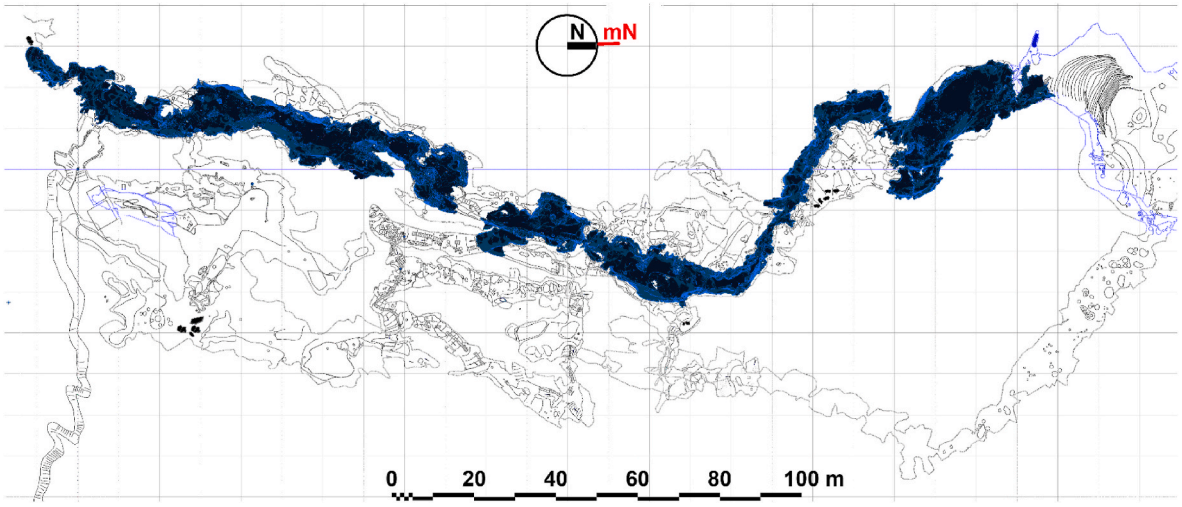

Fig. 5. Mobile LiDAR 3D mesh overlaying the cave's map.
Source: Own elaboration based on Juan Mayoral-Valsera's map (Mayoral Valsera et al., 2017).

occlusions for comprehensive modelling.

SfM, an accessible and cost-effective alternative to traditional 3D scanning methods, produces high-resolution models from multiple photographs and their position calculation through feature triangulation. Unlike TLS or SLS, SfM uses any camera, making it ideal for researchers with limited resources and inaccessible environments. However, the computationally intensive SfM requires well-executed photographic surveying (Di Angelo et al., 2024) and tools, such as total stations, for alignment and scaling. Its reliance on images can limit its effectiveness in low-light conditions, like caves, and may complicate capturing flat surfaces without sufficient oblique and peripheral images (Di Iorio et al., 2024). In speleological environments, geometrical complexity may require using different lenses, focal lengths, or image sizes (Arza-García et al., 2019). However, SfM has been effectively used in cave settings, including underwater sites for studying marine sponge diversity (Pulido Mantas et al., 2023) and in ice caves for monitoring changes in ice deposits (Securo et al., 2022).

This technological and scientific evolution reveals integrated approaches in cave documentation, where technical precision aids research and conservation. Specialised methods for rock art offer targeted data collection for specific areas but may lose some broader spatial context compared to full-cave digitisation.

2.2. 3D modelling of heritage sites

Current 3D modelling approaches in heritage documentation encompass 2D imagery, TLS point clouds, and SLS or SfM 3D meshes. While 2D data is limited in capturing depth and spatial relationships, TLS models provide greater detail and accuracy, though they require extensive processing for effective heritage representation (Fortunato et al., 2024; Barazzetti et al., 2015b; Antón et al., 2019). Meanwhile, SfM creates detailed and photorealistic 3D meshes that accurately represent heritage sites.

Heritage models based on TLS 3D meshes derive from the Scan-to-Mesh process (Lei et al., 2024), closely related to the Scan-to-BIM approach for HBIM. 3D reconstruction of scan data can be performed using triangulation methods in software, e.g., Leica Cyclone 3DR (Leica Geosystems, 2024), or recognised open-source programmes such as CloudCompare (Girardeau-Montaut, 2016) or MeshLab (Cignoni et al., 2008), utilising the Screened Poisson Surface Reconstruction algorithm (Kazhdan and Hoppe, 2013). The smoothing and simplification levels affect the quality and quantity of triangles in the mesh (Antón et al., 2019), allowing for varied resolutions. High-polygon models can be optimised through re-meshing and retopology using tools similar to Instant Meshes (Jakob et al., 2015), resulting in lower polygon count (low-poly) meshes that improve model handling. Moreover, quadrilateral meshes outperform triangle-based products for capturing sharp features, and enhance texture mapping and compression (Lei et al., 2024; Docampo-Sanchez and Haimes, 2019).

2.3. Smartphone LiDAR's potential in cave digitisation

Recent advancements in smartphone LiDAR technology provide an effective alternative for creating 3D digital models in archaeology and speleology, especially in confined or hard-to-reach areas. Its portability and ease of use allow users with limited resources to document and share digital representations. Although TLS and SfM offer higher accuracy, mobile LiDAR is valuable in cave archaeology due to its accessibility. It has been used to interact with Palaeolithic rock art (Rivero et al., 2024), but also when the cave surface has been vandalised with graffiti (Jessy Kartini et al., 2023).

Delving into affordability, Table 1 offers an overview of the cost range of TLS and smartphone LiDAR (focusing on the Apple iPhone as in this research or iPad) equipment and software for point cloud processing, including basic versions and comprehensive suites, but excluding advanced engineering options.

Smartphone LiDAR is effective for documenting small areas and can complement high-resolution models when accuracy is required. However, its use as the sole technique for full-cave digitisation is yet to be evaluated. An accuracy analysis against a total station point network and TLS point cloud data is needed to determine its suitability for preserving and disseminating archaeological and speleological heritage.

3. Research aim

This research aimed to democratise the use of low-cost mobile LiDAR 3D scanning in archaeology and speleology. To do this, specific objectives were set.

- To document a room, sector or panel of great interest in La Pileta Cave, with numerous morphological details and rock art samples.
- To evaluate the suitability of this built-in smartphone LiDAR technology against TLS and total station measurements in such a complex case study.

Table 2
Evaluation of mobile LiDAR accuracy using the three applications: a) Polycam, b) 3d Scanner app, and c) MetaScan. *P.* accounts for point, *Dist.* for distance, and *(0,0,0)* is the origin of the coordinate system, whereas the mean error is expressed in metres and percentage (%), *Sd* is the standard deviation (error) in metres and percentage (%), and *CoV* accounts for the coefficient of variation (standard deviation divided by the mean).

a) Polycam

P. ID	Total station point coordinates (m)			Mobile LiDAR 3D mesh vertex coordinates (m)			Difference in coordinates (m)			Error (m)	Dist. to (0,0,0) (m)	Error/Dist. (%)
	X	Y	Z	X	Y	Z	X	Y	Z			
24	−18.67	235.64	22.99	−18.67	235.64	22.99	0.00	0.00	0.00	0.00	0.00	0.00
23	−14.66	227.19	25.85	−14.31	227.18	25.89	−0.35	0.01	−0.03	0.35	9.78	3.56
22	−19.06	220.58	24.61	−18.64	220.40	24.56	−0.42	0.18	0.05	0.46	15.06	3.06
21	−7.25	209.35	24.35	−6.74	209.94	24.31	−0.51	−0.59	0.04	0.78	28.70	2.72
20	−11.58	197.66	24.44	−10.92	198.14	24.34	−0.65	−0.48	0.11	0.82	38.66	2.11
19	−15.86	196.86	23.84	−15.44	197.04	23.82	−0.42	−0.18	0.02	0.46	93.28	0.49
18	−14.19	182.15	21.27	−13.29	182.87	21.14	−0.90	−0.72	0.13	1.16	53.70	2.15
17	−7.25	182.49	21.19	−6.37	183.24	21.07	−0.88	−0.75	0.12	1.16	54.39	2.14
16	−1.86	176.59	18.48	−0.94	177.10	18.30	−0.92	−0.51	0.18	1.07	61.56	1.73
15	9.05	174.40	21.55	9.81	174.63	21.32	−0.76	−0.23	0.23	0.83	67.23	1.23
14	15.61	168.38	20.82	16.38	168.34	20.55	−0.76	0.04	0.27	0.81	75.52	1.07
13	20.07	168.20	20.28	20.71	168.05	20.02	−0.64	0.15	0.26	0.71	77.82	0.91

Mean 'Error (m)'	**Mean 'Error/Dist. (%)'**	**Standard deviation 'Error (m)'**	**St. dev. 'Error/Dist. (%)'**	**CoV 'Error (m)'**	**CoV 'Error/Dist. (%)'**
0.72	1.76	0.35	**1.06**	**0.49**	**0.60**

b) 3d Scanner app

P. ID	Total station point coordinates (m)			Mobile LiDAR 3D mesh vertex coordinates (m)			Difference in coordinates (m)			Error (m)	Dist. to (0,0,0) (m)	Error/Dist. (%)
	X	Y	Z	X	Y	Z	X	Y	Z			
24	−18.67	235.64	22.99	−18.67	235.64	22.99	0.00	0.00	0.00	0.00	0.00	0.00
23	−14.66	227.19	25.85	−14.97	226.98	25.89	0.31	0.21	−0.04	0.38	9.78	3.87
22	−19.06	220.58	24.61	−19.87	220.66	24.76	0.81	−0.08	−0.15	0.83	15.06	5.51
21	−7.25	209.35	24.35	−8.22	209.42	24.58	0.97	−0.07	−0.23	1.00	28.70	3.48
20	−11.58	197.66	24.44	−12.93	197.62	24.71	1.36	0.04	−0.27	1.38	38.66	3.58
19	−15.86	196.86	23.84	−16.79	197.81	24.11	0.93	−0.95	−0.27	1.36	93.28	1.46
18	−14.19	182.15	21.27	−14.28	181.96	21.85	0.09	0.19	−0.58	0.62	53.70	1.15
17	−7.25	182.49	21.19	−8.77	182.50	21.62	1.53	−0.01	−0.43	1.59	54.39	2.92
16	−1.86	176.59	18.48	−3.22	176.59	18.87	1.36	0.00	−0.40	1.42	61.56	2.31
15	9.05	174.40	21.55	8.01	174.39	22.04	1.04	0.01	−0.48	1.15	67.23	1.71
14	15.61	168.38	20.82	15.04	168.30	21.28	0.57	0.08	−0.47	0.74	75.52	0.98
13	20.07	168.20	20.28	19.67	168.21	20.75	0.40	−0.01	−0.47	0.62	77.82	0.79

Mean 'Error (m)'	**Mean 'Error/Dist. (%)'**	**Standard deviation 'Error (m)'**	**St. dev. 'Error/Dist. (%)'**	**CoV 'Error (m)'**	**CoV 'Error/Dist. (%)'**
0.92	2.31	0.48	1.59	0.52	0.69

c) MetaScan

P. ID	Total station point coordinates (m)			Mobile LiDAR 3D mesh vertex coordinates (m)			Difference in coordinates (m)			Error (m)	Dist. to (0,0,0) (m)	Error/Dist. (%)
	X	Y	Z	X	Y	Z	X	Y	Z			
24	−18.67	235.64	22.99	−18.67	235.64	22.99	0.00	0.00	0.00	0.00	0.00	0.00
23	−14.66	227.19	25.85	−14.44	227.16	25.90	−0.22	0.03	−0.05	0.23	9.78	2.31
22	−19.06	220.58	24.61	−18.50	220.71	24.58	−0.56	−0.13	0.03	0.57	15.06	3.81
21	−7.25	209.35	24.35	−6.61	210.22	24.28	−0.63	−0.87	0.07	1.08	28.70	3.76
20	−11.58	197.66	24.44	−11.10	197.96	24.26	−0.47	−0.30	0.18	0.59	38.66	1.52
19	−15.86	196.86	23.84	−15.45	197.18	23.63	−0.41	−0.32	0.21	0.56	93.28	0.60
18	−14.19	182.15	21.27	−13.92	182.53	21.02	−0.27	−0.38	0.25	0.53	53.70	0.98
17	−7.25	182.49	21.19	−7.05	182.65	20.92	−0.19	−0.16	0.27	0.37	54.39	0.68
16	−1.86	176.59	18.48	−1.87	176.59	18.10	0.01	0.00	0.38	0.38	61.56	0.62
15	9.05	174.40	21.55	9.05	173.95	21.20	0.00	0.45	0.35	0.57	67.23	0.85
14	15.61	168.38	20.82	15.68	167.52	20.47	−0.07	0.86	0.35	0.93	75.52	1.23
13	20.07	168.20	20.28	19.59	167.24	20.00	0.48	0.96	0.28	1.11	77.82	1.43

Mean 'Error (m)'	**Mean 'Error/Dist. (%)'**	**Standard deviation 'Error (m)'**	**St. dev. 'Error/Dist. (%)'**	**CoV 'Error (m)'**	**CoV 'Error/Dist. (%)'**
0.58	**1.48**	**0.33**	1.22	0.57	0.82

Source: Own elaboration.

4. Materials and methods

4.1. Site of data collection

The chosen case study area of La Pileta Cave, described in the Introduction, included the Galería de la Reina Mora, leading to the also scanned Baño de la Reina Mora, the adjacent Sala del Pez, and the closest sector of the Gran Sima to the latter (Fig. 1).

4.2. Equipment used

The research methodology, mainly based on 3D recording, reconstruction, and validation, addresses the case study's geometry capture using two different LiDAR devices: an Apple iPhone 15 Pro smartphone and a tripod-mounted TLS unit, the BLK360 G1 by Leica Geosystems (Leica Geosystems, 2018a).

Since the iPhone 12 Pro, Apple has implemented a LiDAR sensor in

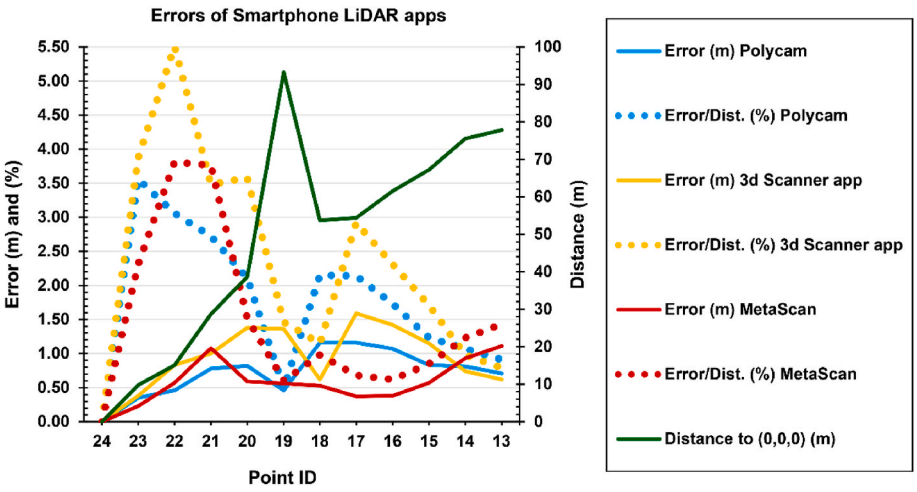

Fig. 6. Errors of smartphone LiDAR applications.
Source: Own elaboration.

'Pro' smartphones and tablets (iPad). The iPhone 15 Pro (Apple Inc, 2023) was used to carry out the mobile LiDAR digitisation of La Pileta. Nevertheless, a mobile application is needed to operate the LiDAR sensor, such as Scaniverse (Toolbox AI Inc, 2020), Polycam (Polycam Inc, 2022), MetaScan (Metafour UK Ltd, 2018), Modelar (Modelar Technologies, 2023), 3d Scanner App (Laan Labs, 2020), CamToPlan (Tasmanic Editions, 2018), or RTAB-Map (Labbe, 2021). Some of them also allow photogrammetry. In this research, the applications Polycam, MetaScan, and 3d Scanner App were used because of their photograph size, the possibility of controlling the voxel size—this determines the mesh resolution—and their simple interface.

Regarding the Leica BLK360, its measurement rate of approximately 360,000 points per second, 60 m scanning range and 3D point accuracy of 4 mm at 10 m distance (Leica Geosystems, 2018a), make it a massive geometric data capture technology for both outdoor and indoor 3D scanning applications.

Finally it is worth describing the two workstations used in this research to process (i) the mobile LiDAR data and (ii) the TLS point cloud.

- (i) Mac Studio: 32 GB M2 Max chip with a 12-core CPU, 30-core GPU, 16-core Neural Engine, and 400 GB/s memory bandwidth;
- (ii) 14-core microprocessor (6 performance cores and 8 efficient cores, with 20 threads) at 5.1 GHz maximum with 24 MB cache; 64 GB DDR4 RAM at 3200 MHz; and a PCIe 4.0 graphics card with 5888 GPU cores, 2.48 GHz graphics clock, and 12 GB 192-bit GDDR6X memory at 21,000 MHz with 504.2 GB/s bandwidth.

4.3. Data collection

4.3.1. Smartphone LiDAR 3D digitisation

4.3.1.1. Illumination. Lighting is crucial for studies in complete darkness. For uniform lighting, an ABS 3D-printed handheld support was ad-hoc developed to hold a smartphone and two Fenix CL28R (Distribucion, 2023) rechargeable lanterns (Fig. 2). These lanterns emit up to 2000 lumens at 160° and feature adjustable colour temperatures between 2700K and 6000K for improved colour rendering on stone surfaces. A 5000 mAh rechargeable battery powers each lantern, and a 20,000 mAh external power bank is included in the support for extended scanning time.

4.3.1.2. 3D recording. The smartphone LiDAR survey may require previous calibration and planning for adequate geometry capture. Key parameters, such as maximum scanning distance and mesh size, must be selected. The iPhone's LiDAR range is about 5 m, but shorter distances can be set (starting at 0.30 m). Lower mesh resolution (e.g., 2.5–4 cm) produces more detail but larger file sizes (over 2 GB), thus complicating high-resolution scans of larger areas. PTC (Vuforia) and Polycam's user guides to creating LiDAR captures provide useful instructions for achieving suitable 3D meshes with Apple's built-in LiDAR devices (PTC Inc, 2023; Polycam Inc, 2023). Following an S pattern, scanning should ensure sufficient overlap and be slow to avoid sudden, uncontrolled equipment movements (Trujillo-Talavera et al., 2024) so that the surface is accurately captured and 3D mesh holes are minimised. Light conditions are also important, so undesired shadows on objects are to be avoided (PTC Inc, 2023). Poor lighting or exceeding the maximum range can cause artefacts and inconsistent data. To minimise distortions, operators should maintain a perpendicular position to the surface and cover the area from multiple angles, re-scanning to fill gaps.

Due to hardware limitations, scans of 2–3-m long should be sought during fieldwork. For a continuous survey, overlapping 15–20-min scans ensures proper orientation and starting heights. 3D Scanner App facilitates this by allowing pauses and resuming, saving drafts for later processing, and alerting when scan capacity reaches 50 %. It automatically closes at 100 % without losing data, easing future processing.

4.3.1.3. Post-processing. Selecting the correct processing system in applications operating the built-in LiDAR sensor is important, as variations in voxel size and mesh quality influence 3D model quality and file size. Large files may require a workstation with at least 32 GB of RAM.

Scan data export formats include.OBJ, .USDZ, and.FBX. For this research, the.OBJ format was chosen because it preserves mesh geometry (Antón et al., 2018), resulting in a compressed (.ZIP) file including the.OBJ file, .JPG textures, and.MTL data. Blender (Blender Foundation, 2024) was chosen to process.OBJ files from La Pileta Cave. Total station Ground control points (GCPs) were established using a Topcon GPT3000N unit (recording range from 1.5 to 250 m and accuracy of 5 mm) by establishing a traverse network (route of stations) along La Pileta's main itinerary. GCPs were flagged on the ground by sticking yellow marks and later recorded using smartphone LiDAR and TLS, to be integrated into the former for accurate positioning. The scanned cave spaces were organised as 'collections' in Blender, with common reference point coordinates identified for aligning the 3D meshes, i.e., ensuring accurate positioning of cave sectors. This permitted quantifying the mobile applications' errors (subsection 5.3). Additionally, the GNSS coordinates of a point outside the cave enable the calculation of depth and XY location for any point in the case study.

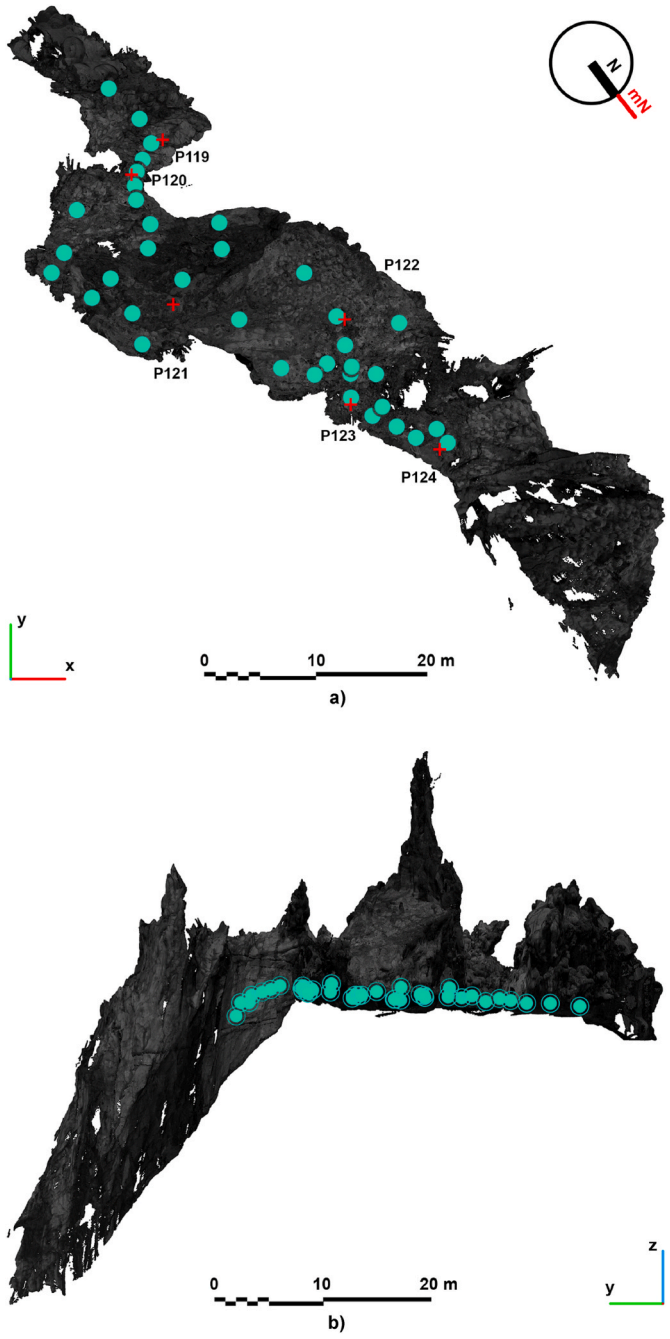

Fig. 7. TLS cloud with the stations' layout: **a)** Top view, with total station GCPs; **b)** Elevation view.
Source: Own elaboration.

Geometrical inconsistencies (artefacts) from 3D surveys, such as floating geometries from accidental recording of operators, water reflections, falling drops, or flying bats, can be removed using the 'lasso' tool in Blender. Lighting was also carefully arranged in Blender through setting and adjusting in-motion light sources along the camera and 'Sun' light for global lighting to minimise dark or overexposed areas and enhance cave feature visibility. Finally, animations and orthophotographs were created to produce detailed cave plans without distortion.

4.3.2. TLS (Terrestrial Laser Scanning)

4.3.2.1. 3D recording. The TLS survey was initially planned using a map, but the positions of some scan stations were adjusted on-site to avoid obstacles like columns and uneven ground. 37 strategically placed stations (Fig. 3) allowed the capture of most of the cave sector's geometry, ensuring no important data was lost in the point cloud. Total station points (GCPs) recorded in the cave itinerary were also scanned to be later used for alignment and verification.

The scanning accuracy was set to 'high' for distances over 10 m and 'medium' for shorter distances, providing range accuracies of 7 mm at 20 m and 4 mm at 10 m, respectively. Although the high dynamic range (HDR) feature extended the survey time, it was activated to enhance image contrast and, therefore, point cloud colour mapping. LED lamps illuminated the surface without obstructing the scanner's field of view to capture cave colours.

4.3.2.2. 3D point cloud processing. The raw scan data were imported into Leica Cyclone Register 360 (Leica Geosystems, 2018b) to align scans in the same coordinate system. This registration process was mostly automated using cloud-to-cloud constraints (scan links), with occasional manual overlaying for better overlap. These manual processes involved identifying recongnisable cave features, mainly speleothems such as columns, stalagmites, and stalactites, to superimpose the different scans; the software's optimisation algorithm achieved the best fit between clouds. The registration results included 165 links, 59 % overlap, 80 % link strength, and a 7-mm group alignment error.

The TLS point cloud was manually segmented to remove unwanted data, including noise, fence segments, railings, and 'no entry' signs. This was performed using CloudCompare (Girardeau-Montaut, 2016), widely used and validated by the scientific community. Two methods were applied for removal: i) manual segmentation to eliminate excess data points, and ii) intensity-based filtering to distinguish points near the stone surface—each point has a different intensity value depending on the colour, material, texture and humidity content of the surface, among others (Antón et al., 2022). These processes helped ensure accurate data for future 3D reconstruction.

Additionally, addressing the cave's uneven lighting during the survey, images taken by the BLK360's built-in camera on each station were processed to enhance texture by adjusting HDR parameters (gamma, brightness, and contrast) using Cyclone Register 360.

5. Results

5.1. Mobile LiDAR scanning

The smartphone LiDAR's 5-m scanning range captures the lower sections of cave walls, where most rock paintings are found. Fig. 4 shows the mobile LiDAR scanning output in the Blender software environment. Fig. 4a displays the 3D mesh of La Pileta's iconic Gran Pez (Big Fish), revealing its triangular structure and texture. The absence of ceiling surfaces and upper wall sections reveals the cave sector's documented geomorphological features (Fig. 4b). After geo-referencing, the 3D mesh was aligned with the cave floor plan (Fig. 5). The main itinerary, from the Cueva de las Vacas to the Gran Sima, is illustrated from south to north, omitting the lower galleries for clarity. To highlight the significance of the smartphone LiDAR survey, a video (https://youtu.be/Tj0RH8ZXtcM) compares the 3D mesh dataset to the human scale, featuring a human figure at the cave entrance for reference. This video covers the itinerary in Fig. 5, several galleries below, and down the Gran Sima.

5.1.1. Smartphone LiDAR's registration accuracy

To evaluate mobile LiDAR's registration accuracy for cave digitisation, the deviation between its 3D meshes and 12 known total station GCPs was quantified for each mobile application used, including statistical descriptors of error distribution such as mean error, standard deviation (error), and coefficient of variation (standard deviation divided by the mean) (Tables 2a, 2b, and 2c). Lower values of these

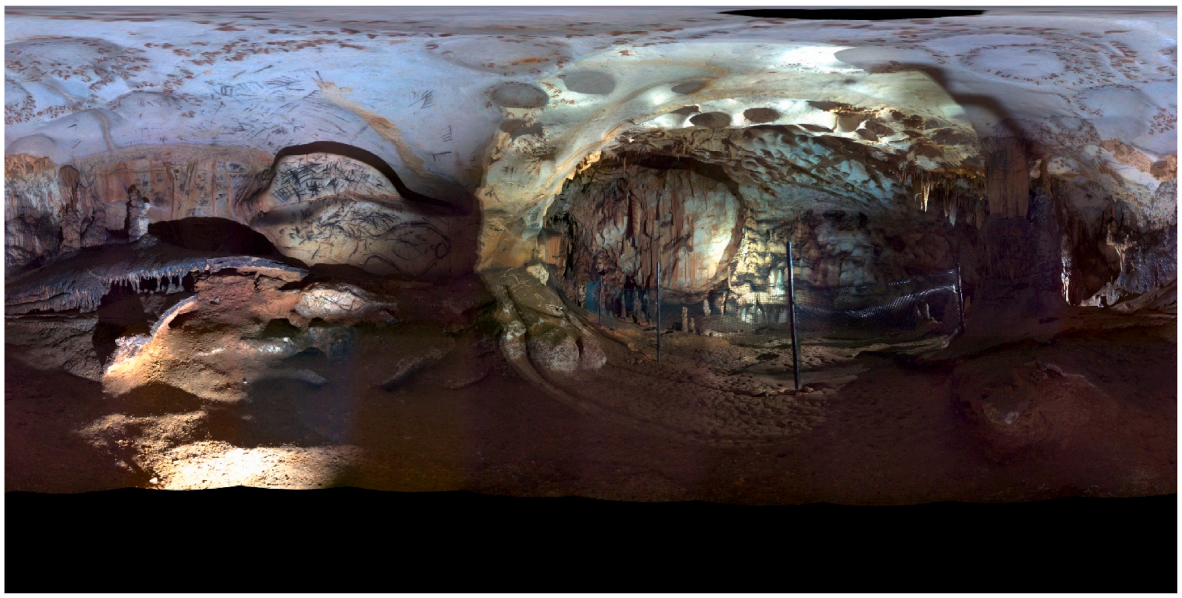

Fig. 8. HDR panorama of the Gran Pez and surrounding paintings.
Source: Own elaboration.

Table 3
Errors in TLS recording in relation to an established itinerary of total station point references (GCPs).

Point ID	XY error (m)	Z error (m)	3D error (m)	Segment (between GCPs)	Distance (m)
119	0.0628	0.0025	0.0629	–	–
120	0.0476	0.0013	0.0476	119–120	9.35
121	0.0206	0.0043	0.0211	120–121	7.94
122	0.0125	0.0049	0.0135	121–122	16.10
123	0.0423	0.0105	0.0436	122–123	12.73
124	0.0655	0.0099	0.0662	123–124	4.36
Mean	0.0419	0.0056	0.0425	**Total**	50.48

Source: Own elaboration.

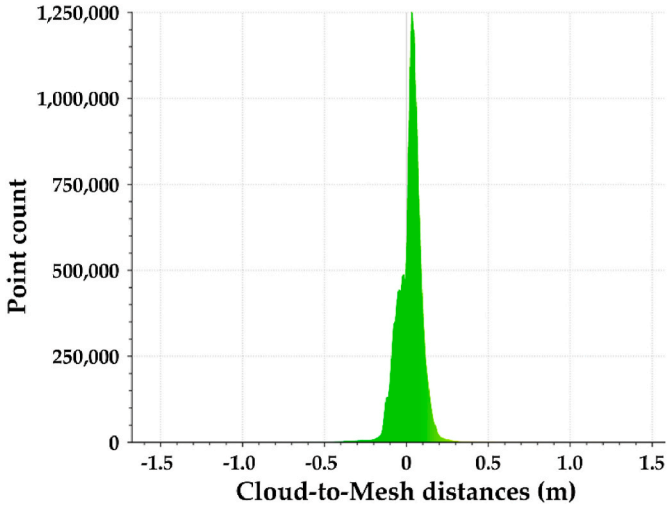

Fig. 9. Validation of mobile LiDAR against TLS. Histogram of points and distance intervals (metres).
Source: Own elaboration.

descriptors indicate better results. Numbers are rounded to two decimal places.

Fig. 6 illustrates the accuracies achieved by each application in relation to the total distance from stations.

Once both the Euclidean distance and weighted error were calculated for each point, the root mean square error (RMSe) was then computed as the square root of the mean of the squared individual errors, providing a global measure of the typical deviation between the datasets. This results in RMSe of 0.79 m and 2.04 m for Polycam app, 1.03 m and 2.77 m for 3d Scanner app, and 0.66 m and 1.89 m for MetaScan, thus reflecting the overall level of agreement between the mobile LiDAR applications and the reference total station data.

Finally, rather than determining the best smartphone survey application, this research highlights mobile LiDAR technology as cost-effective for cave 3D reconstruction. However, compared to other applications, MetaScan shows fewer errors, lower standard deviation, and reduced coefficient of variation. While Polycam exhibits less data dispersion, MetaScan offers greater accuracy and consistency in its 3D mesh output.

5.2. TLS digitisation: 3D point cloud data

The TLS survey generated a point cloud of over 1 billion points, totalling 1,014,918,585, which represents the cave surface geometry (Fig. 7a). An elevation view of the point cloud reveals the scale of the Gran Sima and the ceilings and shafts in the Sala del Pez relative to the human-scale TLS stations (Fig. 7b). Only the closest part of the Gran Sima visible from its balcony, near the gallery leading to the Sala del Pez, was scanned.

Finally, photographs taken during the TLS survey allowed Cyclone Register 360 to produce spherical images, completing the dome (the scanner's field of view). Fig. 8 shows an HDR panorama of Sala del Pez, the cave space named after the remarkable (fish) painting on the wall.

5.3. Technology validation

5.3.1. TLS data

Before deeming TLS infallible, its validation against total station GCPs in the cave sector was essential. They were stored as a separate point cloud, which would later be aligned with those references identified in the TLS data by point-pair picking in CloudCompare. Its cloud-to-cloud (C2C) tool was next used to compute the distances between the two clouds (total station GCPs and TLS GCPs), yielding a 19.6-mm

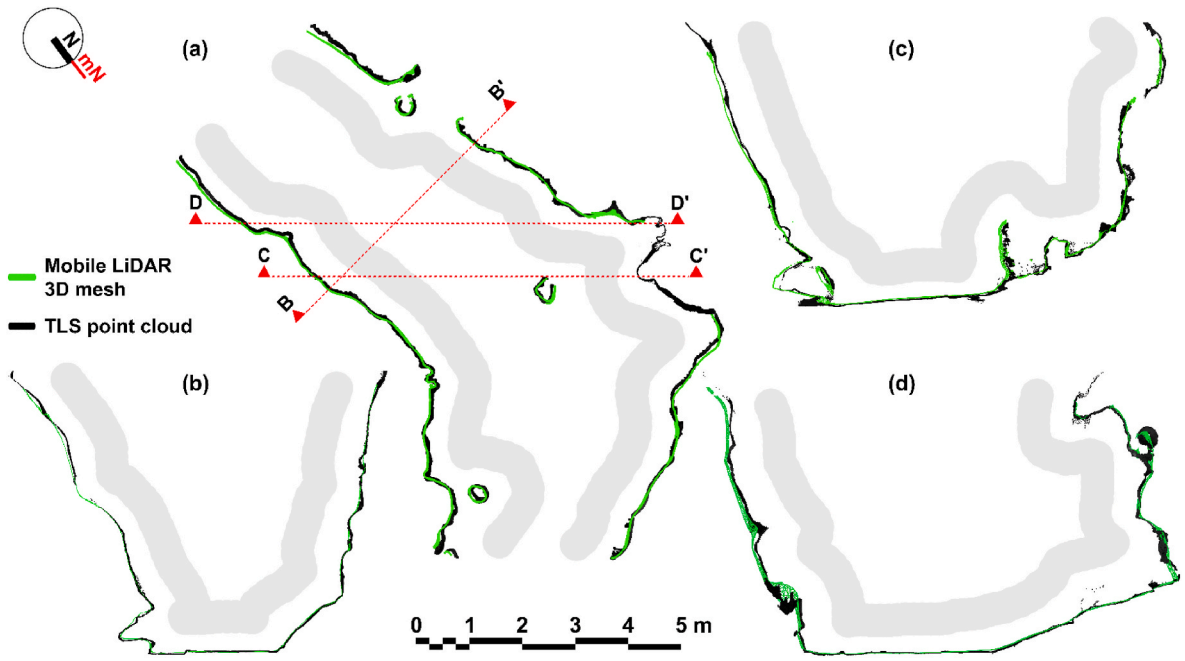

Fig. 10. Sections of the Galería de la Reina Mora: a) horizontal section; b) cross-section B-B'; c) and d) diagonal sections C-C′ and D-D′, respectively. Source: Own elaboration.

standard deviation. Table 3 presents the TLS cloud errors in top view, elevation, and 3D, along with the distances of the total station network stretches within the cave sector.

5.3.2. *Mobile LiDAR 3D reconstruction*

Here, the accuracy of smartphone LiDAR is compared to the cave sector's TLS data. The iPhone geometry of the Galería de la Reina Mora was imported into CloudCompare to be aligned with the corresponding TLS data. Next, the latter needed segmentation to remove, by polygon fencing, the geometry beyond the mobile LiDAR's 5-m range for a rigorous geometrical analysis. The C2C distances were computed, yielding a 22-mm mean distance between the segmented TLS cloud (over 144 million points) and the smartphone 3D mesh (circa 360,000 faces and 336,000 vertexes), with a 71-mm standard deviation. Fig. 9 illustrates the quantitative data deriving from the point deviation analysis between both techniques.

It is also worth conducting a visual comparison between the data from both technologies. To this end, horizontal (a) and vertical (b–d) sections of the TLS point clouds and the smartphone LiDAR 3D meshes are overlaid (Fig. 10), correspondingly. The horizontal section (a) was created 1.25 m above the ground level of the Galería de la Reina Mora; section (b) is a cross-section of this space; and sections (c) and (d) are diagonal sections spaced 1 m apart from each other. For clarity, a general outline in grey is inserted for each section.

6. Discussion

This paper demonstrates that TLS is effective for capturing geometric data in cave archaeology and speleology. The analysis showed an average shift of 4 mm (nearly negligible in the Z-axis) and a 2-mm standard deviation error in the Leica BLK360 data, compared to total station measurements over 50 m in La Pileta Cave. Also, the TLS point cloud registration in this complex karstic landscape yielded a 7-mm error. Consequently, TLS was also deemed suitable for validating smartphone LiDAR for cave digitisation. Additionally, the HDR panoramas produced using TLS are Virtual Reality (VR)-ready for a more realistic, immersive exploration of La Pileta.

The known 5-m scanning range of mobile LiDAR restricts the recording of spatial references at greater heights and may complicate global registration. However, this research showed a low deviation between the 3D mesh and the reference GCPs (Table 2). Notably, the MetaScan application for iPhone exhibited lower mean error and less standard deviation than other applications. Smartphone LiDAR geometry shows an average deviation of 22 mm from the TLS data, with a 71-mm standard deviation. This point data dispersion indicates possible registration issues since some areas place mobile LiDAR geometry above and below TLS points, while others accurately overlap in both datasets. Regions with a more accurate fit compensate for those with greater deviations. Further inspection of the surface geometry revealed that the largest deviations tend to occur on isolated speleothems and on smoother surfaces, where the lack of relief reduces the scanner's ability to reconstruct the 3D geometry reliably. Conversely, in areas with more prominent features and greater surface relief, the mobile LiDAR performed more accurately, as these features provide additional reference points that improve the registration and alignment process. Such pronounced relief is common in these karstic cave contexts, further supporting the suitability of smartphone LiDAR for documenting these environments.

Each technique has its advantages and disadvantages; however, there are several aspects in which mobile LiDAR surpasses TLS in cave environments. Digitisation becomes challenging in spaces such as narrow passages where the operator cannot stand, crouch, or kneel; in shafts above or below the cave's relative ground level; or in areas with low and/or complex ceilings prone to laser beam occlusion. Using TLS in these locations, if possible at all, is often impractical, as setting stations every metre is not feasible for large-scale digitisation. Here, the manoeuvrability of smartphone LiDAR proves advantageous, enabling access to areas that are otherwise difficult to reach. Nonetheless, TLS requires only the operator to press a button after setting up each station. In contrast, smartphone LiDAR is less automated and more physically demanding, as it involves manually scanning all desired areas while carrying the equipment throughout the cave.

Lighting is another key factor when comparing both techniques in complete darkness. Unlike the mobile LiDAR's 3D-printed mount with built-in, fixed-position lamps that provide more uniform illumination, arranging suitable lighting for a TLS survey is not straightforward.

Lamps can be attached to the tripod to illuminate visible cave surfaces, but the parallax between these light sources and the LiDAR causes shadows that require additional lamps positioned outside the scanner's field of view. Furthermore, it is not only the lamps themselves, hidden within the surroundings, but also the light they cast on the ground or surfaces on which they are placed that must be managed. Additionally, light is more intense on nearby surfaces and weaker on distant ones, resulting in overexposure and underexposure, respectively, in the TLS texture or spherical photograph. Uneven lighting also complicates achieving uniform colour in TLS imagery. All light sources should share the same colour temperature (a neutral 4000K is recommended).

In terms of post-processing, both techniques require aligning their own 3D datasets with each other and with established GCPs and spatial references defined by cave features such as speleothems. TLS processing software often includes more automated tools for this purpose, such as cloud-to-cloud registration, which can make the alignment process more efficient.

Considering all the above, Antón et al. (2024b) described as-is geometries as triangle-based 3D models created to match original remote sensing data closely. These 'deformed' models accurately represent the complex shapes of heritage assets, avoiding idealisations, and support analysis, restoration, digital preservation, and dissemination through VR technologies. Despite the higher accuracy of TLS, this research focuses on smartphone LiDAR 3D meshes, regarded as as-is models, and therefore, deemed valid for reconstructing global shapes in archaeology and speleology.

7. Conclusions

Cave topography is expected to undergo significant advancements in the future, driven by the adoption of smartphone and professional-grade LiDAR systems, requiring more costly but highly precise instruments. Although they can be used independently, their combination could overcome the limitations of each and produce qualitative and quantitative better cave documentation. Smartphone LiDAR for caves provides relatively accurate and reliable data to represent their morphologies despite the range and registration limitations discussed in this study. Additionally, incorporating texture data into the digital models enhances their utility and interpretative value in cave archaeology and speleology.

Both the traditional laser metres used in caves and total stations could complement LiDAR technology to determine long distances in large chambers, shafts, or high ceilings. However, the dense TLS point clouds—comprising millions of points—constitute an exceptional resource for detailed topographical and morphological analyses of caves. This data can be seamlessly integrated with other systems, including photogrammetry, altimetry, and GPS, to produce comprehensive and multidimensional cave representations. As a remote sensing technology, smartphone LiDAR reduces the subjectivity involved in traditional hand-drawn cave representations, replacing artistic interpretation with data-driven precision. While this may diminish the creative aspects of traditional topography, it offers enhanced reliability and an extensive dataset that benefits various scientific disciplines.

Particularly, textured 3D cave models, with higher image quality and visual appeal in smartphone LiDAR against TLS, enable the localisation of archaeological, geological, or biological details, among others. For example, individual rock art panels can be separately scanned and accurately superimposed onto the broader cave model as an independent item with its spatial coordinates. This facilitates diverse analyses, such as the shape characterisation of paintings, their distribution, or geological investigations into gallery inclinations or mineral deposits. Therefore, this LiDAR combination has great potential in cave research.

Finally, it is worth depicting the advantages and disadvantages of smartphone LiDAR and making recommendations on its use in this context.

7.1. Benefits of mobile LiDAR in caves

- Being carried by the speleologist, the smartphone LiDAR system enables scanning of difficult-to-reach areas, such as narrow or concealed spaces or within shafts.
- Occlusions are avoided since there is no need to set multiple stations as required by TLS.
- Considering the mobile LiDAR's field of view and limited range, it is easier for operators to stay out of the scanner's sight so as not to be recorded.
- There is no need for a stable and even base to secure the scanner, unlike TLS.
- The lower resolution of mobile LiDAR's 3D meshes against TLS benefits data handling and processing.
- The cost of the smartphone used is notably lower than the TLS device analysed (BLK360 G1).

7.2. Detected limitations

- iPhone LiDAR's scanning range (5 m) is severely limited compared to the BLK360 G1 (up to 60 m).
- Smartphone LiDAR 3D meshes exhibit significantly lower accuracy and, therefore, resolution compared to TLS clouds and 3D meshes built from them.
- The error detected in the mobile-LiDAR–TLS deviation analysis for validation could indicate registration issues of the former.

7.3. Recommendations

The combination of TLS and smartphone LiDAR ensures complete cave digitisation, leveraging the greater range and stability of the former and the manoeuvrability, higher quality texture and lower cost of the latter.

Regarding the use of these technologies, TLS is widely employed in fields such as architecture and archaeology under a well-established protocol. In caves, where specific and unfavourable conditions often apply, it is worth producing a series of recommendations on using smartphone LiDAR to obtain suitable results while ensuring the health and safety of operators.

7.3.1. Procedural

Considering mobile devices' current memory and processing capacity limitations, their efficiency and accuracy should be tested for extensive 3D scanning. Future advancements are expected to allow capturing larger datasets, making external batteries advisable. Optimising tools like handheld supports for mobile scanning is critical. The 3D-printed device in this study evolved from a two-handed support, which limited manoeuvrability.

Key scanning factors include the distance and angle to surfaces, mesh resolution, and lighting. Operators must adjust the 3D survey configuration to achieve the desired accuracy and quality. Additionally, the scope of scanning should be carefully considered, as larger areas create larger file sizes, hindering data handling and visualisation.

7.3.2. Lighting

This research highlights the need for suitable lighting conditions and the avoidance of unwanted shadows. It recommends that (i) wide-beam lanterns be symmetrically mounted on smartphones with adjustable colour and brightness, and (ii) helmet-mounted lights be turned off to avoid interference with scanning lighting. This adjustment provides the right 'warmth' for image capture while reducing overexposure from reflections, which is common in light-coloured geological formations like limestone. Furthermore, it minimises interference from white or bluish light sources, which is crucial for preserving ancient cave paintings. Adjusting colour temperature and brightness is essential, as mobile LiDAR scans map coloured images onto 3D geometry. Future research

could investigate colour correction with this technology.

7.3.3. Safety measures

Cave exploration entails risks, also during 3D scanning in complex environments. It is essential to secure mobile scanning equipment and use appropriate caving systems. When using descender devices on shafts or ramps, they must be locked at each session, requiring recording pauses. Recording while ascending is preferable since two anchoring points reduce the need for a locking knot, but care must be taken to avoid the hand device during scanning. Applying common sense is crucial when navigating different cavern formations and obstacles. Additionally, having a companion is highly recommended to enhance safety and assist.

CRediT authorship contribution statement

Daniel Antón: Writing – review & editing, Writing – original draft, Visualization, Validation, Supervision, Software, Resources, Project administration, Methodology, Investigation, Funding acquisition, Formal analysis, Data curation, Conceptualization. **Juan Mayoral-Valsera:** Writing – review & editing, Writing – original draft, Visualization, Validation, Supervision, Software, Resources, Project administration, Methodology, Investigation, Formal analysis, Data curation, Conceptualization. **María Dolores Simón-Vallejo:** Writing – review & editing, Writing – original draft, Supervision, Resources, Project administration, Methodology, Investigation, Funding acquisition, Conceptualization. **Rubén Parrilla-Giráldez:** Writing – review & editing, Writing – original draft, Methodology, Investigation. **Miguel Cortés-Sánchez:** Writing – review & editing, Writing – original draft, Supervision, Resources, Project administration, Methodology, Investigation, Funding acquisition, Conceptualization.

Funding

This work is linked to the projects US-1264079 (Proyectos I+D+i FEDER Andalucía, 2014–2020) and CROSSYM (PID2023-151553NB-I00) developed by the HUM1089-PAMSUR Group. This work was also supported by the VI Plan Propio de Investigación y Transferencia of Universidad de Sevilla, Spain [reference VIPPIT-2020-II.5].

Declaration of competing interest

The authors declare that they have no known competing financial interests or personal relationships that could have appeared to influence the work reported in this paper.

Acknowledgements

The authors wish to thank the Bullón family, managers of La Pileta, for their support and facilities, as well as the Marbelli Speleological Section (Marbella, Málaga) and the Pluto Sports Club (Seville) for logistical support in the field.

Appendix A. Supplementary data

Supplementary data to this article can be found online at https://doi.org/10.1016/j.jas.2025.106330.

References

Alshawabkeh, Y., Baik, A., 2023. Integration of photogrammetry and laser scanning for enhancing scan-to-HBIM modeling of Al ula heritage site. Herit. Sci. 11, 147. https://doi.org/10.1186/s40494-023-00997-2.

Antón, D., Medjdoub, B., Shrahily, R., Moyano, J., 2018. Accuracy evaluation of the semi-automatic 3D modeling for historical building information models. Int. J. Architect. Herit. 12, 790–805. https://doi.org/10.1080/15583058.2017.1415391.

Antón, D., Pineda, P., Medjdoub, B., Iranzo, A., 2019. As-Built 3D heritage city modelling to support numerical structural analysis: application to the assessment of an archaeological remain. Remote Sens. 11, 1276. https://doi.org/10.3390/rs11111276.

Antón, D., Carretero-Ayuso, M.J., Moyano-Campos, J., Nieto-Julián, J.E., 2022. Laser scanning intensity fingerprint: 3D visualisation and analysis of building surface deficiencies. In: Bienvenido-Huertas, D., Moyano-Campos, J. (Eds.), New Technol. Build. Constr. Springer Nature Singapore, Singapore, pp. 207–223. https://doi.org/10.1007/978-981-19-1894-0_12.

Antón, D., Amaro-Mellado, J.-L., Al-Habaibeh, A., 2024a. Investigating the use of 3D laser scanning to detect damaged features in heritage buildings. In: Tejedor Herrán, B., Bienvenido-Huertas, D. (Eds.), Diagnosis Herit. Build. by Non-destructive Tech. Elsevier, pp. 219–244. https://doi.org/10.1016/B978-0-443-16001-1.00009-7.

Antón, D., Amaro-Mellado, J.-L., Rico-Delgado, F., Díaz-Cañete, P., 2024b. Exploring the accessibility of deformed digital heritage models. In: Tejedor Herrán, B., Bienvenido-Huertas, D. (Eds.), Diagnosis Herit. Build. by Non-destructive Tech. Elsevier, pp. 275–302. https://doi.org/10.1016/B978-0-443-16001-1.00011-5.

Apple Inc, 2023. iPhone 15 pro, IPhone. https://support.apple.com/es-es/111829. (Accessed 15 June 2023).

Arias, F., Enríquez, C., Jurado, J.M., Ortega, L., Romero-Manchado, A., Cubillas, J.J., 2022. Use of 3D models as a didactic resource in archaeology. A case study analysis. Herit. Sci. 10, 112. https://doi.org/10.1186/s40494-022-00738-x.

Artec 3D, 2017. Artec leo, 3D scanners. https://www.artec3d.com/es/portable-3d-scanners/artec-leo. (Accessed 26 March 2024).

Arza-García, M., Gil-Docampo, M., Ortiz-Sanz, J., 2019. A hybrid photogrammetry approach for archaeological sites: block alignment issues in a case study (the roman camp of A cidadela). J. Cult. Herit. 38, 195–203. https://doi.org/10.1016/j.culher.2019.01.001.

Backhaus, J., De Arriba López, V., Maboudi, M., Bestmann, U., Gerke, M., 2024. Combining UAV-Based photogrammetry and structured light scanning to support the structural health monitoring of concrete structures. E-J. Nondestruct. Test. 29, 1–10. https://doi.org/10.58286/29797.

Bakker, W.H., Feringa, W., Gieske, A.S.M., Gorte, B.G.H., Grabmaier, K.A., Hecker, C.A., Horn, J.A., Huurneman, G.C., Janssen, L.L.F., Kerle, N., van der Meer, F.D., Parodi, G.N., Pohl, C., V Reeves, C., van Ruitenbeek, F.J., Schetselaar, E.M., Tempfli, K., Weir, M.J.C., Westinga, E., Woldai, T., 2009. Principles of Remote Sensing, fourth ed. The International Institute for Geo-Information Science and Earth Observation (ITC), Enschede, The Netherlands https://webapps.itc.utwente.nl/librarywww/papers_2009/general/principlesremotesensing.pdf.

Balestrieri, M., Valmori, I., Montuori, M., 2024. UAS and TLS 3D data fusion for built cultural heritage assessment and the application for st. Catherine monastery in Ferrara, Italy. Int. Arch. Photogram. Rem. Sens. Spatial Inf. Sci. XLVIII-M–4, 9–16. https://doi.org/10.5194/isprs-archives-XLVIII-M-4-2024-9-2024.

Barazzetti, L., Banfi, F., Brumana, R., Oreni, D., Previtali, M., Roncoroni, F., 2015a. HBIM and augmented information: towards a wider user community of image and range-based reconstructions. Int. Arch. Photogramm. Remote Sens. Spat. Inf. Sci. - ISPRS Arch. XL-5/W7, 35–42. https://doi.org/10.5194/isprsarchives-XL-5-W7-35-2015.

Barazzetti, L., Banfi, F., Brumana, R., Gusmeroli, G., Previtali, M., Schiantarelli, G., 2015b. Cloud-to-BIM-to-FEM: structural simulation with accurate historic BIM from laser scans. Simulat. Model. Pract. Theor. 57, 71–87. https://doi.org/10.1016/j.simpat.2015.06.004.

Bassier, M., Bonduel, M., Derdaele, J., Vergauwen, M., 2020. Processing existing building geometry for reuse as linked data. Autom. ConStruct. 115, 103180. https://doi.org/10.1016/j.autcon.2020.103180.

Blender Foundation, Blender, 2024.

Breuil, H., Obermaier, H., Verner, W., 1915. La Pileta À Benaojan (Malaga) (Espagne). Institut de Paleontologie Humaine, Monaco.

Brumana, R., Oreni, D., Cuca, B., Binda, L., Condoleo, P., Triggiani, M., 2014. Strategy for integrated surveying techniques finalized to interpretive models in a byzantine church, mesopotam, Albania. Int. J. Architect. Herit. 8, 886–924. https://doi.org/10.1080/15583058.2012.756077.

Chiabrando, F., Sammartano, G., Spanò, A., 2016. Historical buildings models and their handling via 3d survey: from points clouds to user-oriented hbim. Int. Arch. Photogramm. Remote Sens. Spat. Inf. Sci. - ISPRS Arch. XLI-B5, 633–640. https://doi.org/10.5194/isprsarchives-XLI-B5-633-2016.

Cignoni, P., Callieri, M., Corsini, M., Dellepiane, M., Ganovelli, F., Ranzuglia, G., 2008. MeshLab: an open-source mesh processing tool. In: Scarano, V., De Chiara, R., Erra, U. (Eds.), Sixth Eurographics Ital. Chapter Conf. The Eurographics Association, Salerno, Italy, pp. 129–136. https://doi.org/10.2312/LocalChapterEvents/ItalChap/ItalianChapConf2008/129-136.

Çömert, R., Özdemir, S., Bilgilioglu, B.B., Alemdag, S., Zeybek, H.I., 2023. 3D data integration for geo-located cave mapping based on unmanned aerial vehicle and terrestrial laser scanner data. Baltica 36, 37–50. https://doi.org/10.5200/baltica.2023.1.4.

Cortés-Sánchez, M., Simón-Vallejo, M.D., 2007. La Pileta (Benaoján, Málaga) cien años después. Aportaciones al conocimiento de su secuencia arqueológica. Sagvntvm Papeles Del Lab. Arqueol. Val 45–63. https://turia.uv.es//index.php/saguntum/article/view/1050/553.

Cortés-Sánchez, M., Simón-Vallejo, M.D., Parrilla-Giráldez, R., Calle-Román, L., 2015. Old panels and new readings. In: Bueno-Ramírez, P., Bahn, P.G. (Eds.), Prehist. Art as Prehist. Cult. Stud. Honour Profr. Rodrigo Balbín-Behrmann. Archaeopress Publishing Ltd, pp. 135–144. https://doi.org/10.2307/j.ctvr43m2m.19.

Cortés-Sánchez, M., Simón-Vallejo, M.D., Martínez Sánchez, R.M., García Borja, P., Bretones García, M.D., Ruiz Borrega, M.P., de la Rubia de Gracia, J.J., Parrilla-Giráldez, R., 2016a. El Neolítico en la Cueva de la Pileta (Benaoján, Málaga). Arch.

Prehist. Levantina 31, 119–136. https://mupreva.org/pub/935/va. (Accessed 24 June 2025).
Cortés-Sánchez, M., Simón-Vallejo, M.D., Morales-Muñiz, A., Lozano Francisco, M.C., Vera Peláez, J.L., Odriozola-Lloret, C., 2016b. La caverna iluminada: una singular lámpara gravetiense arroja luz sobre el arte parietal de la cueva de La Pileta (Benaoján, Málaga). Trab. Prehist. 73, 115–127. https://doi.org/10.3989/tp.2016.12166.
Cortés-Sánchez, M., Morales-Muñiz, A., Jiménez-Espejo, F., Évora, M., Simón-Vallejo, M. D., García-Alix, A., Martínez Aguirre, A., Riquelme-Cantal, J.A., Odriozola-Lloret, C. P., Parrilla-Giráldez, R., Álvarez-Lao, D.J., 2017. Multi-purpose fossils? The reappraisal of an Elephas antiquus molar from El pirulejo (Magdalenian; Córdoba, Spain). Archaeol. Anthropol. Sci. 9, 1287–1303. https://doi.org/10.1007/s12520-016-0324-1.
Cortés-Sánchez, M., Simón-Vallejo, M.D., Parrilla-Giráldez, R., Calle-Román, L., Mayoral-Valsera, J., Odriozola-Lloret, C.P., Macías-Tejada, S., Esparza Sainz, L., 2018a. Cueva de La Pileta (Benaoján, Málaga). In: Handpas Manos Del Pasado Catálogo Represent. Manos En El Arte Rupestre Paleolítico La Península Ibérica, Consejería De Cultura E Igualdad, pp. 477–490.
Cortés-Sánchez, M., Riquelme-Cantal, J.A., Simón-Vallejo, M.D., Parrilla Giráldez, R., Odriozola, C.P., Calle Román, L., Carrión, J.S., Monge Gómez, G., Rodríguez Vidal, J., Moyano Campos, J.J., Rico Delgado, F., Nieto Julián, J.E., Antón García, D., Martínez-Aguirre, M.A., Jiménez Barredo, F., Cantero-Chinchilla, F.N., 2018b. Pre-Solutrean rock art in southernmost Europe: evidence from Las Ventanas Cave (Andalusia, Spain). PLoS One 13, e0204651. https://doi.org/10.1371/journal.pone.0204651.
Cortés-Sánchez, M., Jiménez-Espejo, F.J., Simón-Vallejo, M.D., Stringer, C., Lozano Francisco, M.C., García-Alix, A., Vera Peláez, J.L., Odriozola, C.P., Riquelme-Cantal, J.A., Parrilla Giráldez, R., Maestro González, A., Ohkouchi, N., Morales-Muñiz, A., 2019. An early Aurignacian arrival in southwestern Europe. Nat. Ecol. Evol. 3, 207–212. https://doi.org/10.1038/s41559-018-0753-6.
Cortés-Sánchez, M., Siles Guerrero, F., Simón-Vallejo, M.D., 2023. La Pileta à Benaoján (Málaga) de H. Breuil, H. Obermaier y W. Verner 120 años después, La Serranía, Cádiz. https://www.laserrania.org/producto/la-pileta-a-benaojan-genesis-edicion-facsimil-y-traducida/.
Dams, M., Dams, L., 1975. Considérations sur les figurations paléolithiques de la caverne de la Pileta (Malaga) par rapport à leur localisation topographique, Préhistoire Ariégeoise Bull. La Société Préhistorique L'Ariège30, pp. 13–28. https://catalogus.cultureelerfgoed.nl/Details/fullCatalogue/200089762. (Accessed 24 June 2025).
Dams, L., Dams, M., 1977a. Iconographie complémentaire de la caverne de la Pileta et considérations sur la Cueva de Las Vacas et le réseau de las Grajas (Malaga) | Rijksdienst voor het Cultureel Erfgoed, Préhistoire Ariégeoise Bull. La Société Préhistorique l'Ariège 32, 67–83. https://catalogus.cultureelerfgoed.nl/Details/fullCatalogue/200070698. (Accessed 24 June 2025).
Dams, M., Dams, L., 1977b. L'Art De La Cueva De La Pileta Essai Sur L'École D'Art Paléolithique Mediterranéenne, Trav, vol. 19. Del'Institut D'Archeologie Préhistorique L' Univ., Toulouse, pp. 39–92.
Dams, L., Dams, M., 1983. Quelques considérations sur l'Art Rupestre Schématique d'Andalousie. Zephyrvs Rev. Prehist. y Arqueol. 36, 187–192, 187. https://revistas.usal.es/uno/index.php/0514-7336/article/view/412. (Accessed 24 June 2025).
Decreto 527/1996, De 17 De Diciembre, Por El Que Queda Delimitado El Ámbito Afectado Por La Declaración De Bien De Interés Cultural, Con La Categoría De Zona Arqueológica, Del Yacimiento Denominado «Cueva De La Pileta», En El Término Municipal De Benaoján, 1996. Boletín Oficial del Estado, Spain. https://www.boe.es/diario_boe/txt.php?id=BOE-A-1997-9605.
Di Angelo, L., Schmitt, A., Rummel, M., Di Stefano, P., 2024. Automatic analysis of pottery sherds based on structure from motion scanning: the case of the Phoenician carinated-shoulder amphorae from Tell el-Burak (Lebanon). J. Cult. Herit. 67, 336–351. https://doi.org/10.1016/j.culher.2024.03.012.
Di Iorio, F., Es Sebar, L., Croci, S., Taverni, F., Auenmüller, J., Pozzi, F., Grassini, S., 2024. The use of virtual reflectance transformation imaging (V-RTI) in the field of cultural Heritage: approaching the materiality of an Ancient Egyptian rock-cut chapel. Appl. Sci. 14, 4768. https://doi.org/10.3390/app14114768.
Distribución, Fénix, 2023. Fenix CL28R: multifuncional linterna exterior, Linternas. https://www.fenixlinternas.com/cl-serie/1508-fenix-cl28r-multifuncional-linterna-exterior-6942870309071.html. (Accessed 15 January 2023).
Docampo-Sanchez, J., Haimes, R., 2019. Towards fully regular quad mesh generation. In: AIAA Scitech 2019 Forum. American Institute of Aeronautics and Astronautics, Reston, Virginia. https://doi.org/10.2514/6.2019-1988.
European Commission's Expert Group on Digital Cultural Heritage and Europeana (DCHE Expert Group), 2020. Basic principles and tips for 3D digitisation of cultural heritage. https://digital-strategy.ec.europa.eu/en/library/basic-principles-and-tips-3d-digitisation-cultural-heritage. (Accessed 24 February 2023).
Fiorini, A., 2022. Scansioni dinamiche in archeologia dell'architettura: test e valutazioni metriche del sensore LiDAR di Apple. Archeol. e Calc. 33, 35–54. https://doi.org/10.19282/ac.33.1.2022.03.
Fortea Pérez, F.J., Fortea Pérez, F.J., 2005. La plus ancienne production artistique du Paléolithique ibérique. In: Broglio, A., Dalmeri, G. (Eds.), Pitture Paleolit. Nelle Prealpivenete Grotta Di Fumane E Riparo Dalmieri, Museo Civico Di Storia Naturale Di Verona, pp. 89–99. Verona, 2005.
Fortunato, G., Frega, F., Lauria, A., Zappani, A.A., 2024. Documenting and analysing to preserve: an integrated approach between laser scanning and Computational Fluid Dynamics. The case study of the column of the temple of Hera Lacinia near Crotone. J. Cult. Herit. 66, 244–253. https://doi.org/10.1016/j.culher.2023.11.020.
Giménez Reyna, S., 1951. La Cueva de la Pileta (Benaoján-Málaga), Monumento Nacional, Instituto de Estudios Malagueños, Malaga. http://bibliotecavirtual.malaga.es/es/estaticos/contenido.cmd?pagina=estaticos/presentacion. (Accessed 24 June 2025).
Giménez Reyna, S., 1958. La cueva de la Pileta (Monumento Nacional), Caja de Ahorros Provincial de Málaga, Málaga. http://bibliotecavirtual.malaga.es/es/estaticos/contenido.cmd?pagina=estaticos/presentacion. (Accessed 6 October 2024).
Giménez Reyna, S., de la Pileta, La Cueva, Nacional, Monumento, 1958. Publicaciones De La Caja De Ahorros Provincial De Málaga, Malaga. https://www.iberlibro.com/Cueva-Pileta-Monumento-Nacional-Gimenez-Reyna/30915202076/bd. (Accessed 24 June 2025).
Gines, J.L.C., Cervera, C.B., 2020. Toward hybrid modeling and automatic planimetry for graphic documentation of the archaeological Heritage: the Cortina family pantheon in the cemetery of Valencia. Int. J. Architect. Herit. 14, 1210–1220. https://doi.org/10.1080/15583058.2019.1597214.
Giordan, D., Godone, D., Baldo, M., Piras, M., Grasso, N., Zerbetto, R., 2021. Survey solutions for 3D acquisition and representation of artificial and natural Caves. Appl. Sci. 11, 6482. https://doi.org/10.3390/app11146482.
Girardeau-Montaut, D., 2016. CloudCompare: 3D point cloud and mesh processing software. Open Source Proj. http://www.danielgm.net/cc/.
González-Aguilera, D., Muñoz-Nieto, A., Gómez-Lahoz, J., Herrero-Pascual, J., Gutierrez-Alonso, G., 2009. 3D digital surveying and modelling of Cave geometry: application to Paleolithic rock art. Sensors 9, 1108–1127. https://doi.org/10.3390/s90201108.
Hichri, N., Stefani, De Luca, Veron, P., 2013. Review of the « As-Built bim » approaches. Int. Arch. Photogramm. Remote Sens. Spat. Inf. Sci. - ISPRS Arch. XL-5/W1, 107–112. https://doi.org/10.5194/isprsarchives-XL-5-W1-107-2013.
Hoffmeister, D., Zellmann, S., Pastoors, A., Kehl, M., Cantalejo, P., Ramos, J., Weniger, G., Bareth, G., 2016. The investigation of the ardales Cave, Spain – 3D documentation, topographic analyses, and lighting simulations based on terrestrial laser scanning. Archaeol. Prospect. 23, 75–86. https://doi.org/10.1002/arp.1519.
Jakob, W., Tarini, M., Panozzo, D., Sorkine-Hornung, O., 2015. Instant field-aligned meshes. ACM Trans. Graph. 34, 1–15. https://doi.org/10.1145/2816795.2818078.
Jessy Kartini, G.A., Gumilar, I., Abidin, H.Z., Yondri, L., Nabil Nugany, M.R., 2023. Stonex F6 and iPad Pro M1 2021 for Cave Graffiti inspection in barong Cave, West Java, Indonesia. IOP Conf. Ser. Earth Environ. Sci. 1127, 012031. https://doi.org/10.1088/1755-1315/1127/1/012031.
Jiang, S., Jiang, C., Jiang, W., 2020. Efficient structure from motion for large-scale UAV images: a review and a comparison of SfM tools. ISPRS J. Photogrammetry Remote Sens. 167, 230–251. https://doi.org/10.1016/j.isprsjprs.2020.04.016.
Jordá Cerdá, F., 1955. Sobre la edad solutrense de algunas pinturas de la cueva de la Pileta (Málaga). Zephyrvs Rev. Prehist. y Arqueol. 6, 131–143. https://revistas.usal.es/uno/index.php/0514-7336/article/view/3682. (Accessed 24 June 2025).
Kartini, G.A.J., Gumilar, I., Abidin, H.Z., Yondri, L., Bramanto, B., Dwisatria, M.I., 2024. 3D model of Pawon Cave: the first prehistoric dwelling discovery in West Java, Indonesia, Digit. Appl. Archaeol. Cult. Herit. 32, e00311. https://doi.org/10.1016/j.daach.2023.e00311.
Kazhdan, M., Hoppe, H., 2013. Screened poisson surface reconstruction. ACM Trans. Graph. 32, 1–13. https://doi.org/10.1145/2487228.2487237.
Laan Labs, 2020. 3d scanner app. https://apps.apple.com/es/app/3d-scanner-app/id1419913995. (Accessed 15 June 2023).
Labbé, M., 2021. RTAB-Map - 3D LiDAR scanner on the app Store. https://apps.apple.com/cd/app/rtab-map-3d-lidar-scanner/id1564774365. (Accessed 15 June 2023).
Lei, Y., Fiorillo, F., Fassi, F., 2024. 3D survey point cloud data as direct rendering assets for visualising complex heritage in virtual applications. Int. Arch. Photogram. Rem. Sens. Spatial Inf. Sci. XLVIII-2/W, 279–286. https://doi.org/10.5194/isprs-archives-XLVIII-2-W4-2024-279-2024.
Leica Geosystems, 2018a. BLK360 G1 laser scanner, scanners. https://leica-geosystems.com/en-GB/products/laser-scanners/scanners/blk360. (Accessed 19 April 2018).
Leica Geosystems, Cyclone REGISTER 360, 2018.
Leica geosystems, cyclone 3DR. Laser Scanning Softw, 2024.
Lerma, J.L., Navarro, S., Cabrelles, M., Villaverde, V., 2010. Terrestrial laser scanning and close range photogrammetry for 3D archaeological documentation: the Upper Palaeolithic Cave of Parpalló as a case study. J. Archaeol. Sci. 37, 499–507. https://doi.org/10.1016/j.jas.2009.10.011.
Liu, X., Shan, Y., Ai, G., Du, Z., Shen, A., Lei, N., 2024. A scientific investigation of the shangfang Mountain Yunshui Cave in Beijing based on LiDAR technology. Land 13, 895. https://doi.org/10.3390/land13060895.
Lozano Bravo, H., Lo, E., Moyes, H., Rissolo, D., Montgomery, S., Kuester, F., 2023. A methodology for cave floor basemap synthesis from point cloud data: a case study of SLAM-based LiDAR at Las Cuevas, Belize, ISPRS Ann. Photogramm. Remote Sens. Spat. Inf. Sci. X-M-1–2023, 179–186. https://doi.org/10.5194/isprs-annals-X-M-1-2023-179-2023.
Luetzenburg, G., Kroon, A., Bjørk, A.A., 2021. Evaluation of the Apple iPhone 12 pro LiDAR for an application in geosciences. Sci. Rep. 11, 22221. https://doi.org/10.1038/s41598-021-01763-9.
Mayoral Valsera, J., 2020. Metodología de exploración y topografía en cavidades con restos arqueológicos. La Experiencia De La Cueva De La Pileta, Boletín La Soc. Española Espeleol. Y Ciencias Del Karst SEDECK, pp. 48–60. https://dialnet.unirioja.es/servlet/articulo?codigo=7945490&info=resumen&idioma=ENG. (Accessed 24 June 2025).
Mayoral Valsera, J., Cortés Sánchez, M., Simón Vallejo, M.D., Gavilán Zaldúa, M., 2017. Sistema híbrido de topografía espeleológica. Su aplicación en la nueva topografía de la Cueva de la Pileta (Benaoján, Málaga). In: Alcalá, A., Berrocal, J.A. (Eds.), Actas Del III Simp. Andaluz Topogr. Espeleológica, Federación Andaluza De Espeleología, pp. 71–78. Málaga.
Medina Alcaide, M.Á., Sanchidrián Torti, J.L., 2015. Los signos integrados de Pileta-E: análisis a diferentes profundidades de campo. In: Medina Alcaide, M.Á., Romero Alonso, A.J., Ruiz Marquéz, R.M., Sanchidrián Torti, J.L. (Eds.), Sobre Rocas Y

Huesos Las Soc. Prehistóricas Y Sus Manifestaciones Plásticas, Patronato De La Cueva De Nerja, pp. 116–129. https://dialnet.unirioja.es/servlet/articulo?codigo=6118345. (Accessed 24 June 2025).
Metafour UK Ltd, 2018. MetaScan. https://apps.apple.com/tz/app/metascan/id6736746811. (Accessed 15 June 2023).
Modelar Technologies, Modelar - 3D LiDAR scanner. https://apps.apple.com/es/app/modelar-3d-lidar-scanner/id1572844190, 2023–. (Accessed 15 June 2023).
Moyano, J.J., Barrera, J.A., Nieto, J.E., Marín, D., Antón, D., 2017. A geometrical similarity pattern as an experimental model for shapes in architectural heritage: a case study of the base of the pillars in the cathedral of Seville and the church of Santiago in Jerez, Spain. Int. Arch. Photogramm. Remote Sens. Spat. Inf. Sci. - ISPRS Arch. XLII-2/W3, 511–517. https://doi.org/10.5194/isprs-archives-XLII-2-W3-511-2017.
Moyes, H., Montgomery, S., 2019. Locating Cave entrances using lidar-derived local relief modeling. Geosciences 9, 98. https://doi.org/10.3390/geosciences9020098.
Murphy, M., McGovern, E., Pavia, S., 2009. Historic building information modelling (HBIM). Struct. Surv. 27, 311–327. https://doi.org/10.1108/02630800910985108.
Nieto, J.E., Moyano, J.J., Rico, F., Antón, D., 2016. Management of built heritage via the HBIM Project: a case of study of flooring and wall tiling. Virtual Archaeol. Rev. 7, 1–12. https://doi.org/10.4995/var.2016.4349.
Oreni, D., 2013. From 3D content models to HBIM for conservation and management of built heritage. In: Murgante, B., Misra, S., Carlini, M., Torre, C.M., Nguyen, H.-Q., Taniar, D., Apduhan, B.O., Gervasi, O. (Eds.), Comput. Sci. Its Appl. – ICCSA 2013. Springer Berlin Heidelberg, Ho Chi Minh City, Vietnam, pp. 344–357. https://doi.org/10.1007/978-3-642-39649-6_25.
Özdemir, E., Erdal, K., Veziroğlu, F., Ateş, S.S., 2022. The use of the backpack LiDAR system in the genarate of 3D models in salt Caves; the example of Tuzluca, igdir, Turkish J. Remote Sens. 4. https://doi.org/10.51489/tuzal.1112140.
Özyeşil, O., Voroninski, V., Basri, R., Singer, A., 2017. A survey of structure from motion. Acta Numer. 26, 305–364. https://doi.org/10.1017/S096249291700006X.
Parrilla Giráldez, R., 2023. El arte paleolítico en el sur de la Península Ibérica. Aplicación de nuevas tecnologías a la documentación. Preservación Y Análisis Del Patrimonio, Universidad De Sevilla. https://hdl.handle.net/11441/143349. (Accessed 24 June 2025).
Pepe, M., Costantino, D., Alfio, V.S., Restuccia, A.G., Papalino, N.M., 2021. Scan to BIM for the digital management and representation in 3D GIS environment of cultural heritage site. J. Cult. Herit. 50, 115–125. https://doi.org/10.1016/j.culher.2021.05.006.
Pietroni, E., Menconero, S., Botti, C., Ghedini, F., 2023. e-Archeo: a pilot national project to valorize Italian archaeological parks through digital and virtual reality technologies. Appl. Syst. Innov. 6, 38. https://doi.org/10.3390/asi6020038.
Polycam Inc., 2022. Polycam - 3D LiDAR scanner. https://apps.apple.com/es/app/polycam-escáner-3d-lidar/id1532482376. (Accessed 15 June 2023).
Polycam Inc., 2023. Creating LiDAR captures. Creat. 3D Model. https://learn.poly.cam/hc/en-us/articles/27419935601940-Creating-LiDAR-Captures. (Accessed 15 June 2023).
PTC Inc., 2023. Using 3D scans, vuforia engine libr. https://developer.vuforia.com/library/vuforia-engine/images-and-objects/model-targets/using-3d-scans/how-create-model-targets-3d-scans/#capturing. (Accessed 1 July 2025).
Pukanská, K., Bartoš, K., Bella, P., Gašinec, J., Blistan, P., Kovanič, Ľ., 2020. Surveying and high-resolution topography of the ochtiná aragonite cave based on TLS and digital photogrammetry. Appl. Sci. 10, 4633. https://doi.org/10.3390/app10134633.
Pulido Mantas, T., Roveta, C., Calcinai, B., Coppari, M., Di Camillo, C.G., Marchesi, V., Marrocco, T., Puce, S., Cerrano, C., 2023. Photogrammetry as a promising tool to unveil marine caves' benthic assemblages. Sci. Rep. 13, 7587. https://doi.org/10.1038/s41598-023-34706-7.
Remondino, F., Campana, S. (Eds.), 2014. 3D Recording and Modelling in Archaeology and Cultural Heritage: Theory and Best Practices. Archaeopress British Archaeological Reports, Oxford. https://www.barpublishing.com/book/3d-recording-and-modelling-in-archaeology-and-cultural-heritage-theory-and-best-practices/. (Accessed 24 June 2025).
Ripoll Perelló, E., 1957. Las representaciones antropomorfas en el arte paleolítico español. Ampurias Rev. Arqueol. Prehist. y Etnogr 167–192. https://dialnet.unirioja.es/servlet/articulo?codigo=9509852. (Accessed 24 June 2025).
Ripoll Perelló, E., 1962. La cronología relativa del Santuario de la cueva de la Pileta y el arte solutrense. In: de Mergelina y Luna, C. (Ed.), Homen. Al Profr. Cayetano Mergelina Murcia, 1961-1962. Universidad de Murcia, Murcia, pp. 739–752.
Riquelme, A., Ferrer, B., Mas, D., 2017. Use of high-quality and common commercial mirrors for scanning close-range surfaces using 3D laser scanners: a laboratory experiment. Remote Sens. 9, 1152. https://doi.org/10.3390/rs9111152.
Rivero, O., Dólera, A., García-Bustos, M., Eguilleor-Carmona, X., Mateo-Pellitero, A.M., Ruiz-López, J.F., 2024. Seeing is believing: an augmented reality application for Palaeolithic rock art. J. Cult. Herit. 69, 67–77. https://doi.org/10.1016/j.culher.2024.07.007.
Ruiz López, J., 2020. Tecnologías actuales al servicio de la documentación, estudio, conservación y divulgación del arte rupestre. In: Viñas i Vallverdú, R. (Ed.), I Jornades Int. D'Art Rupestrede L'Arc Mediterrani La Península Ibèrica. Xxè Aniversari La Declar. Patrim. Mund. Museu Comarcal de la Conca de Barberà, Montblanc, pp. 341–373.
Sanchidrián Torti, J.L., 1985. Informe sobre la documentación de las manifestaciones parietales prehistóricas de la Cueva de la Pileta (Benaoján, Málaga). In: Dirección General De Bienes Culturales - Consejería De Cultura De La Junta De Andalucía. Junta de Andalucía, Seville. Anu. Arqueol. Andalucía, 1985 - II Act. Sist. Inf. y Memorias, Consejería de Cultura. http://hdl.handle.net/20.500.11947/14523.
Sanchidrián Torti, J.L., 1986. Arte rupestre: La Cueva de la Pileta, hoy. Rev. Arqueol. 7, 34–44. https://dialnet.unirioja.es/servlet/articulo?codigo=6796217. (Accessed 24 June 2025).
Sanchidrián Torti, J.L., Muñoz Vivas, V.E., 1990. Cuestiones sobre las manifestaciones parietales post-paleolíticas en la cueva de La Pileta (Benaoján, Málaga). Zephyrvs Rev. Prehist. y Arqueol. 43. http://hdl.handle.net/10366/71447. (Accessed 24 June 2025).
Sanchidrián Torti, J.L., Muñoz Vivas, V.E., 1991. Cueva de La Pileta, arte rupestre post-paleolítico. Rev. Arqueol. 12, 10–19. https://dialnet.unirioja.es/servlet/articulo?codigo=2832201. (Accessed 24 June 2025).
Sanchidrián Torti, J.L., 1997. Propuesta de la secuencia figurativa en la Cueva de la Pileta. In: Fullola Pericot, J.M., Soler i Masferrer, N. (Eds.), El Món Mediterrani Després Del Pleniglacial (18000-12000 BP) Col·Loqui, Banyoles 1995. Museu d'Arqueologia de Catalunya, pp. 411–430. Girona. https://dialnet.unirioja.es/servlet/articulo?codigo=7562090. (Accessed 24 June 2025).
Sanchidrián Torti, J.L., Márquez, A.M., Valladas, H., Tisnérat-Laborde, N., 2001. Dates Directes Pour L'Art Rupestre D'Andalousie (Espagne). Int. Newsl. Rock Art. 15–19.
Securo, A., Forte, E., Martinucci, D., Pillon, S., Colucci, R.R., 2022. Long-term mass-balance monitoring and evolution of ice in caves through structure from motion–multi-view stereo and ground-penetrating radar techniques. Prog. Phys. Geogr. Earth Environ. 46, 422–440. https://doi.org/10.1177/03091333211065123.
Shao, W., Vijayarangan, S., Li, C., Kantor, G., 2019. Stereo visual inertial LiDAR simultaneous localization and mapping. In: 2019 IEEE/RSJ Int. Conf. Intell. Robot. Syst., pp. 370–377. https://doi.org/10.1109/IROS40897.2019.8968012. IEEE, Macau.
Simeone, D., Cursi, S., Toldo, I., Carrara, G., 2014. B(H)IM - built heritage information modelling - extending BIM approach to historical and archaeological heritage representation. In: Fusion, Proc. 32nd Int. Conf. Educ. Res. Comput. Aided Archit. Des. Eur. Ecaade Conf., pp. 613–622. Newcastle upon Tyne. https://cumincad.architexturez.net/doc/oai-cumincadworks-id-ecaade2014-204. (Accessed 10 June 2017).
Simón-Vallejo, M.D., Parrilla-Giráldez, R., Macías-Tejada, S., Calle-Román, L., Mayoral-Valsera, J., Cortés-Sánchez, M., 2021. Cueva de La Pileta y las representaciones de manos en el arte paleolítico del sur de Iberia. In: Bea, M., Domingo, R., Mazo, C., Montes, L., Rodanés, J.M. (Eds.), La Mano La Prehist. Homen. a Pilar Utrilla Miranda. Prensas de la Universidad de Zaragoza, Zaragoza, pp. 341–360. https://hdl.handle.net/11441/111561. (Accessed 24 June 2025).
Simón-Vallejo, M.D., Parrilla-Giráldez, R., Macías-Tejada, S., Odriozola-Lloret, C.P., Mayoral-Valsera, J., Cortés-Sánchez, M., 2024. La Pileta (Benaoján, Málaga). Una aproximación interdisciplinaral conocimiento del arte paleolítico del sur de Iberia. In: García-Bustos, M., Rivero Vilá, O. (Eds.), Arte, Simbolismo Y Soc. En La Prehist. Nuevos Descub. Interpret. Y Métodos, pp. 66–70. https://doi.org/10.5281/zenodo.14036200. García-Bustos, Miguel, Salamanca.
Smith, P.J., 2009. A "Splendid Idiosyncrasy": Prehistory at Cambridge 1915-50. University of Michigan Press, Ann Arbor, MI. https://doi.org/10.30861/9781407304304.
Šupinský, J., Kaňuk, J., Nováková, M., Hochmuth, Z., 2022. LiDAR point clouds processing for large-scale cave mapping: a case study of the Majko dome in the Domica Cave. J. Maps 18, 268–275. https://doi.org/10.1080/17445647.2022.2035270.
Tan, K., Cheng, X., 2017. Specular reflection effects elimination in terrestrial laser scanning intensity data using Phong model. Remote Sens. 9, 853. https://doi.org/10.3390/rs9080853.
Tan, K., Zhang, W., Shen, F., Cheng, X., 2018. Investigation of TLS intensity data and distance measurement errors from target specular reflections. Remote Sens. 10, 1077. https://doi.org/10.3390/rs10071077.
CamToPlan, Tasmanic Editions, 2018. https://apps.apple.com/es/app/camtoplan-medir-distancias/id1292176208. (Accessed 15 June 2023).
Toolbox AI Inc, 2020. Scaniverse - 3D scanner. https://apps.apple.com/es/app/scaniverse-3d-scanner/id1541433223. (Accessed 15 June 2023).
Trujillo-Talavera, A., Valverde-Cantero, D., González-Arteaga, J., 2024. Precisión del escáner LIDAR de dispositivos apple para toma de datos en edificación. An. Edif. 10, 75–80. https://doi.org/10.20868/ade.2024.5476.
Tysiac, P., Sieńska, A., Tarnowska, M., Kedziorski, P., Jagoda, M., 2023. Combination of terrestrial laser scanning and UAV photogrammetry for 3D modelling and degradation assessment of heritage building based on a lighting analysis: case study—St. Adalbert Church in Gdansk, Poland. Herit. Sci. 11, 53. https://doi.org/10.1186/s40494-023-00897-5.
Ulvi, A., 2021. Documentation, Three-Dimensional (3D) modelling and visualization of cultural heritage by using Unmanned Aerial Vehicle (UAV) photogrammetry and terrestrial laser scanners. Int. J. Rem. Sens. 42, 1994–2021. https://doi.org/10.1080/01431161.2020.1834164.
Wang, Y., Bi, W., Liu, X., Wang, Y., 2025. Overcoming single-technology limitations in digital heritage preservation: a study of the LiPhoScan 3D reconstruction model. Alex. Eng. J. 119, 518–530. https://doi.org/10.1016/j.aej.2024.12.095.
Werbrouck, J., Pauwels, P., Bonduel, M., Beetz, J., Bekers, W., 2020. Scan-to-graph: semantic enrichment of existing building geometry. Autom. ConStruct. 119, 103286. https://doi.org/10.1016/j.autcon.2020.103286.
Wright, W., 1916. The Art of the Cave 1. Nature 98, 51–52. https://doi.org/10.1038/098051a0.
Xue, F., Wu, L., Lu, W., 2021. Semantic enrichment of building and city information models: a ten-year review. Adv. Eng. Inform. 47, 101245. https://doi.org/10.1016/j.aei.2020.101245.
Zhang, C., Chen, J., Li, P., Han, S., Xu, J., 2024. Integrated high-precision real scene 3D modeling of karst cave landscape based on laser scanning and photogrammetry. Sci. Rep. 14, 20485. https://doi.org/10.1038/s41598-024-71113-y.